Decadal trends in photosynthetic capacity and leaf area index inferred from satellite remote sensing for global vegetation types

Paul B. Alton, Geography Dept., Swansea University, SA2 8PP, UK.
p.alton@swansea.ac.uk +44(0)1792 295069

1 Abstract

In the face of a mounting diversity of experimental, satellite and ground-based observations, it is becoming necessary to simulate *all* changes associated with vegetation (phenological, structural, physiological and biochemical) and to understand the links between them. In this respect, global land-surface models are an indispensible tool. These models require, above all, a temporally and spatially explicit parameterisation of light- and Rubisco-limited photosynthetic capacity in order to simulate photosynthesis accurately. The current study carries out a novel retrieval of these quantities by combining the standard satellite products of Leaf Area Index (LAI), from the Moderate Resolution Imaging Spectroradiometer (MODIS), with a hyperspectral index of total canopy chlorophyll concentration from the MEdium Resolution Imaging Spectrometer (MERIS). Monthly values of photosynthetic capacity are retrieved for the period 2002-2012 for global 0.5° landpoints and made available to the community. We examine the decadal trends in both photosynthetic capacity and LAI in order to ascertain biochemical and structural responses of vegetation to environmental change. The main conclusion is that these trends, if sustained, are of a sufficient magnitude to vie in importance with other environmental factors which affect vegetation productivity and carbon uptake (e.g. CO_2 fertilisation and climate). The decadal trends for Rubisco-limited photosynthetic capacity, which tend to be negative, depend more on plant functional type than latitude, suggesting that biochemical change, like physiological response (e.g. owing to CO_2 fertilisation), might best be monitored in terms of vegetation type rather than climate zone. We record an LAI trend which, globally, is flat (-0.2±0.4% per decade) and, for the (mid-)northern latitudes, is much smaller (1.5-2.7% per decade) than that inferred by previous authors for Normalised Difference Vegetation Index (NDVI) during the 1980s (9-13%).

Keywords

carbon cycle, land-surface modelling, photosynthetic capacity, leaf area index, Moderate Resolution Imaging Spectroradiometer (MODIS), remote-sensing, MEdium Resolution Imaging Spectrometer (MERIS)

2 Introduction

Several landmark measurements reveal that the productivity of global vegetation is changing, although many details of the mechanisms remain elusive:

1. Remotely sensed NDVI (see Tab. 1 for acronyms used frequently in the text) reveals for the 1980s both an advancing spring (phenological change) and an increasing peak in productivity for northern latitudes (lat) $> 40^{\circ}$ (Myneni et al 1997). The latter change is generally attributed to structural change (e.g. increased leaf area) but biochemical change (e.g. greater absorption of sunlight through leaf pigment change) cannot be excluded.

2. An increasing amplitude in the seasonal global atmospheric CO_2 concentration ($[CO_2]$; Keeling et al 1996). This is generally interpreted as enhanced primary productivity in the high northern latitudes (Graven et al 2013; Forkel et al 2016), although an increase in carbon release during the dormant season as respiration cannot be totally excluded (Prentice et al 2000; Graven et al 2013).

3. An increase in both net leaf carbon uptake and ecosystem net primary productivity owing to increasing $[CO_2]$ in Free-air CO_2 enrichment (FACE) experiments (Ainsworth & Long 2005; IPCC 2013). This "CO_2 fertilisation" appears, however, to vary according to Plant Function Type (PFT), with forests affected most (Norby et al 2005; Luo et al 2006). Furthermore, it is unclear whether the enhancement is sustained, given that nitrogen (N) is often limiting, even in temperate zones of high anthropogenic N-deposition (Townsend et al 1996; Nadelhoffer et al 1999; Cleveland et al 2013; but see Lloyd 1999). Paradoxically, there is also an expectation that active leaf-N (Rubisco and chlorophyll) may actually decline owing to acclimation to higher $[CO_2]$ and diversion of plant-N to enhanced root growth (Prentice et al 2000; Ainsworth & Long 2005; Leakey et al 2009).

In the face of these observations, it is becoming necessary to understand and simulate all changes associated with vegetation (phenological, structural, physiological and biochemical) as well as the interactions among them.

Global land-surface models, when supported by increasing field and satellite observations, are an invaluable tool in this respect and some of the latest models even couple the carbon and N cycles, so that changes in active leaf-N, for example, influence carbon assimilation (Zaehle et al 2010; Smith et al 2014). Above all, most land-surface and carbon models require a temporally and spatially explicit parameterisation of both light- and Rubisco-limited photosynthetic capacity in order to simulate photosynthesis accurately (Dang et al 1998; Bonan et al 2011). The advent of airborne and satellite hyperspectral instruments make this possible *via* remote sensing (Grace et al 2007). However, many hyperspectral vegetation studies have hitherto focussed primarily on sun-induced fluoresence (which relates to chlorophyll) in agricultural areas (Zhang et al 2014; Guanter et al 2014) or the correlation of multiple optical and near-infrared wavelengths to leaf chemistry at *regional* level (Smith et al 2002; Serbin et al 2012; Ollinger et al 2013). A more comprehensive study is called for, covering both natural and anthropogenic (e.g. agricultural) global PFTs, where N-limitations may differ.

The main purpose of the present study is to produce temporally resolved global maps of light- and Rubisco-limited photosynthetic capacity (J^{25}_{max} and V^{25}_{cmax}, respectively, for a standard leaf temperature of 25°C), which are suitable for land-surface model parameterisation, as well as revealing spatial and temporal trends in active leaf-N. This is achieved by the novel step of combining LAI, inferred from MODIS broadband reflectance, with a hyperspectral index sensitive to ground chlorophyll concentration, derived from MERIS (operational period 2002-2012). Both datasets are satellite-based and quasi-global. The photosynthetic capacity (biochemical) trend will be compared with structural (LAI) change. Studies of remotely sensed LAI trend are fairly scant (Mao et al 2013; Zhu et al 2016), although the strongly related Normalised Difference Vegetation Index (NDVI) has been subject to trend analysis (Myneni et al 1997; Zhou et al 2001; Zhang et

al 2007; Los 2013). Given its importance, few studies explicitly compare the contemporary period with the large increase in NDVI found by Myneni et al (1997) for northern latitudes during the 1980s (but see Los 2013).

Specific objectives of the current study are as follows:

1. To determine the magnitude and sign of biochemical (photosynthetic capacity) and structural (LAI) decadal trends and to compare them with the impact of CO_2 fertilisation on vegetation productivity.
2. To ascertain whether these trends correlate more strongly with latitude (as a proxy for climate) rather than with vegetation type.
3. To test whether the large increases in NDVI recorded during the 1980s (Myneni et al 1997) are sustained and manifest themselves in LAI increases for the period 2002-2012.
4. To relate the spatial distribution of photosynthetic capacity to both vegetation type and latitude, comparing the retrieved global range with recent field-based compilations such as TRY (Kattge et al 2009).
5. To make monthly 0.5° global maps of light- and Rubisco-limited photosynthetic capacity available to the community and thus considerably improve the land-surface model parameterisation for two of the most influential parameters determining carbon-exchange at the land-surface. The current parameterisation, based on general time-invariant values, is inadequate and often inconsistent (Rogers 2014).

3 Material and Methods

The methodology is introduced below in the following sequence:

1. conceptual background to the retrieval (§3.1);
2. input satellite datasets (MTCI from MERIS and LAI from MODIS)(§3.2);
3. protocol for retrieval (§3.3);
4. sensitivity analysis (§3.4);

3.1 Conceptual Background

The retrieval combines the following 4 steps (see Alton 2017 for detailed equations and a schematic overview):

1. Leaf measurements (discussed below) indicate a linear or saturating relationship between maximum electron transport for the light reaction (J^{25}_{max}) and leaf chlorophyll content (Chl);
2. The sum of Chl integrated over canopy LAI (i.e. chlorophyll concentration per unit ground) is detected with the hyperspectral index MTCI which has recently been calibrated against ground measurements of chlorophyll (Dash et al 2010; Vuolo et al 2012).
3. A fairly tight near-linear empirical relationship is observed between J^{25}_{max} and V^{25}_{cmax}, consistent with the optimisation of active leaf-N over a diverse range of C_3 plants (e.g. Wullschleger 1993; Meir et al 2002; Walker et al 2014).

4. Thus, the chlorophyll concentration per unit ground, derived from remote sensing in step 2 above, can be related to Rubisco-limited photosynthetic capacity summed vertically over the canopy. Equivalently, using the observed exponential vertical decline in active leaf-N (Carswell et al 2000; Lewis et al 2000; Meir et al 2002), we can retrieve V_{cmax}^{25} at the canopy top ($V_{cmax}^{25,toc}$) from known values of MTCI and canopy LAI.

The above 4 steps yield:

$$a_{mtci}\mathbf{MTCI} - b_{mtci} = \int_0^{\mathbf{LAI}} \frac{a_{wull}}{a_{chl}}[1 - \frac{b_{chl}}{a_{wull}} - exp(\frac{-V_{cmax}^{25,toc} exp(k_{rub}L)}{b_{wull}})]dL \quad (1)$$

where input satellite quantities have been highlighted in bold. Integration takes place over cumulative leaf area (L) from the canopy top to a depth into the canopy. Active leaf-N (chlorophyll and Rubisco) declines exponentially with L according to a vertical N-allocation parameter, k_{rub} (Hirose & Werger 1987), which is assigned an average observed value of 0.15 (Carswell et al 2000; Lewis et al 2000; Meir et al 2002). The other terms in Eq. 1 are coefficients in the biochemical relations summarised in steps 1-3 above (Tab. 2). Thus, the terms a_{wull} and b_{wull} follow from a least-squares fit between J_{max}^{25} and V_{cmax}^{25} using numerous observations compiled by Wullschleger (1993). The coefficients a_{mtci} and b_{mtci}, which relate MTCI to chlorophyll concentration per unit ground, are calibrated by ground measurements (Dash et al 2010).

The coefficients a_{chl} and b_{chl} in Eq.1, which relate J_{max}^{25} to leaf chlorophyll content (Tab. 2), were originally assigned values of 240 μmol s^{-1} g^{-1} and 24 μmol m^{-2} s^{-1}, respectively, in a pioneer retrieval of $V_{cmax}^{25,toc}$ at FLUXNET sites (Alton 2017). This corresponded to a best-fit between only 6 measurements of J_{max}^{25} and Chl and by pooling several PFTs. The current study extends this method by fitting each PFT separately and incorporating more data, though Chl is now inferred rather than measured. Thus, paired measurements of J_{max}^{25} and leaf-N are extracted from the database of Walker et al (2014; n=254). Leaf-N is converted to leaf chlorophyll content using a ratio which is conservative over most PFTs viz. leaf-N/Chl = 4.12$\pm$0.32 g m^{-2} [g m^{-2}]$^{-1}$ (Evans 1989). To bolster these data, paired measurements of J_{max} and leaf-N are taken from the TRY database (Kattge et al 2009; n=536). Although J_{max} within TRY is not necessarily at the standard temperature of 25°C, where these data overlap with Walker et al (e.g. for non-tropical broadleaf forest), the relationship is not significantly different ($p<0.05$). The fitting of a_{chl} and b_{chl} is conducted separately for $Chl \leq 0.4$ and $Chl > 0.4$. For $Chl \leq 0.4$, the best fit line is forced through the origin (b_{chl}=0), under the assumption that electron transport is zero when chlorophyll is absent (Fig. 1 and Tab. 3).

Given the division of the J_{max}^{25}-Chl relation into two linear functions, Eq. 1 is integrated in two parts, according to the cumulative leaf area at which Chl falls below 0.4 g m^{-2} (active leaf-N declines with depth through the canopy). We favour a bimodal linear fit to J_{max}^{25}-Chl, over a hyperbolic or exponential function, to render Eq. 1 tractable. Substituting best-fit values for a_{wull}, b_{wull}, a_{mtci} and b_{mtci} into Eq. 1 yields:

$$0.616MTCI - 0.700 = \int_0^{LAI} \frac{428}{a_{chl}(PFT)}[1 - \frac{b_{chl}(PFT)}{428} - exp(\frac{-V_{cmax}^{25,toc} exp(-0.15L)}{158})]dL \quad (2)$$

where the best-fit values for a_{chl} and b_{chl} are given in Tab. 3 according to PFT.

Eq. 1 only applies to PFTs with a C_3 photosynthetic pathway because the relationship J_{max}^{25}-V_{cmax}^{25} is undocumented for C_4 vegetation. However, numerous leaf-based observations (e.g. Wullschleger 1993; Meir et al 2002; Walker et al 2014) suggest an optimisation of active leaf-N for C_3 vegetation between maximum electron transport (relating to chlorophyll) and Rubisco-limited reduction. We assume this optimisation holds for C_4 vegetation so that V_{cmax}^{25} assumes values which are appropriate to match electron transport in full light. The presence of bundle sheath chloroplasts in C_4 leaves leads to an efficiency enhancement in CO_2 reduction, with respect to the C_3 pathway, by inhibiting photorespiration (Jones 1992). From equations C1

and C2 in Sellers et al (1996), based on a Farquhar-type leaf photosynthesis model (Farquhar et al 1980), this efficiency factor ($F_{photoresp}$) follows as:

$$F_{photoresp} = \frac{C_i + K_c(1 + \frac{O_2}{K_o})}{C_i - C_p} \tag{3}$$

where C_i is the leaf-internal CO_2 pressure, O_2 is the leaf-internal oxygen pressure, K_c and K_o are the Michaelis-Menten constants, and C_p is the compensation point (all for C_3 vegetation). For C_i = 25-28 Pa (Wong et al 1979; Collatz et al 1992; Campbell & Norman 1998) and C_p = 4 Pa (Collatz et al 1991), $F_{photoresp} = 3.62 \pm 0.33$. For C_4 leaves, therefore, we assume that V_{cmax}^{25} is reduced by a factor 3.62 compared to C_3 leaves with the same capacity for electron transport (as expressed by J_{max}^{25}). Measurements confirm that the Rubisco content is several times lower in C_4 leaves compared to C_3 leaves for the same levels of chlorophyll (Sage et al 1987; Evans 1989). Our modification for C_4 leaves is implemented by reducing b_{wull} in Eq. 2 from 158 to 44.

Our retrieval method is subject to quite a few uncertainties, particularly for C_4 vegetation where the relationship between J_{max}^{25} and V_{cmax}^{25} is not measured. Therefore, we check against Houborg et al (2013) who exploit empirical relationships between active and total foliar N, recorded for both C_3 and C_4 crops, in order to derive V_{cmax}^{25} from leaf chlorophyll content. Thus:

$$V_{cmax}^{25,toc}(houb) = \frac{a_{houb}(0.114 \times MTCI - 0.158) + 0.15 b_{houb} LAI}{1 - exp(-0.15 LAI)} \tag{4}$$

where the empirical constants a_{houb} and b_{houb} are 253 and -27, respectively, for C_3 crops and 98.8 and -8.6, respectively, for C_4 crops (see Appendix A for detail).

3.2 Input Datasets for Retrieval

3.2.1 MTCI from MERIS

The steep gradient in spectral reflectance between the red and near-infrared domains (690-750 nm), known as the red edge derivative, provides a strong probe of foliar chemistry and in particular chlorophyll content (Middleton et al 2003). This is exploited in the MERIS Terrestrial Chlorophyll Index (MTCI):

$$MTCI = \frac{R_{753.75} - R_{708.75}}{R_{708.75} - R_{681.25}} \tag{5}$$

where R is reflectance at the subscript wavelength given in nanometres (Curran et al 2007). The filters are narrow (Fig.2) to quantify the gradient in the red-edge which is known to correlate strongly (R^2=0.6-0.8) with canopy chlorophyll concentration over crops and the chlorophyll content of broadleaves and needle-leaves (Dash & Curran (2007); Dash et al (2010)).

We access the standard MTCI product (Curran et al 2007) from the NERC Earth Observation Data Centre (NEODC) which provides monthly values at a spatial resolution of 0.04° for the global ice-free land-surface over a 10 yr MERIS operational period (6/2002-3/2012). Pixels are mean-averaged to the spatial resolution of the MODIS global LAI maps (0.5°) introduced below.

Note that the LAI retrieved by MODIS and other satellite detectors (e.g. AVHRR and SPOT) is based on broadband optical and near-infrared reflectance rather than the narrowband filters used by MTCI to quantify the gradient in the red-edge. The two sets of filters (MERIS and MODIS) are independent although the inference of both chlorophyll concentration and LAI relies on the relatively high reflectance in the near-infrared compared to the optical domain (Fig. 2). Note that the MTCI derived from broadleaf and

needleleaf laboratory spectra correlates strongly (R^2=0.6-0.8) with measured chlorophyll content (Dash & Curran 2007). Furthermore, for both crops and non-tropical broadleaf forest, the chlorophyll concentration per unit ground, sampled within the MERIS footprint, correlates strongly (R^2=0.74–0.80) with MTCI (Dash et al 2010; Vuolo et al 2012). Several authors demonstrate a linear response of MTCI to high chlorophyll concentration per unit ground and, therefore, the index is sensitive to dense foliage ($\leq$ 4.5 g m^{-2}; Peng et al 2017).

3.2.2 LAI from MODIS

Global LAI maps at 0.5° resolution (typically used in land-surface and climate modelling) are created for the MTCI-available period (2002-2012) by extracting and mean averaging 0.5 km pixels in the standard 8-day MCD15A2H (C6) MODIS product. The latest C6 LAI product corrects for long-term detector degradation present in previous (e.g. C4 and C5) releases (Yan et al 2016; Zhang et al 2017). Only pixels of good quality are selected i.e. main algorithm, no significant cloud and >50% detectors working (Yang et al 2006). To minimise noise in the phenology timeseries to be created (De Kauwe et al 2011), the global 0.5° maps are averaged temporally using a median 32-day moving window, except for the tropics where persistent cloud (Zhao et al 2005) necessitates selection of the maximum LAI value over a moving 48-day window (Ryu et al 2011). We require a monthly value of LAI, synchronised with MTCI, in order to retrieve $V_{cmax}^{25,toc}$. Therefore, for each 0.5° global location, LAI is extracted via bilinear interpolation from the two temporally averaged global 8-day images which straddle the middle of the month in question.

3.3 Retrieval Protocol

We derive monthly global 0.5° $V_{cmax}^{25,toc}$ using Eq. 2 with modification for C_4 vegetation as indicated in §3.1. Owing to the double exponential on the right side of this equation, $V_{cmax}^{25,toc}$ is solved by forward-modelling. Thus, prior to retrieval, we create a PFT-specific look-up table for the right side of Eq. 2 for narrowly separated values of LAI (ΔLAI = 0.01 m^2 m^{-2}) and $V_{cmax}^{25,toc}$ ($\Delta V_{cmax}^{25,toc}$ = 1 μmol m^{-2} s^{-1}). For each global pixel, observed monthly MTCI is substituted into the left of Eq. 2 and the resulting value is matched against integrals in the look-up table according to the LAI for that month. This yields $V_{cmax}^{25,toc}$. The monthly retrieval is carried out for the entire MERIS operational period (June 2002 to March 2012). Top-of-canopy light-limited photosynthetic capacity ($J_{max}^{25,toc}$) is derived from $V_{cmax}^{25,toc}$ using the empirical fit between J_{max}^{25} and V_{cmax}^{25}, with substitution of a_{wull} and b_{wull} (Tab. 2). Note, however, that our results will focus on $V_{cmax}^{25,toc}$, given the near-proportional relationship between J_{max}^{25} and V_{cmax}^{25}.

For thin or sparse vegetation, MTCI has greater sensitivity to the background (soil) reflectance, which increases the error in retrieved $V_{cmax}^{25,toc}$. This is particularly noticeable for LAI <0.5 m^2 m^{-2} and the retrieval is only undertaken for monthly LAI greater than this threshold. Furthermore, for LAI $\geq$1.5 m^2 m^{-2}, more than half the downwelling shortwave radiation is incident on leaves rather than the ground, assuming a turbid leaf canopy with a spherical leaf angular distribution (Campbell & Norman 1998: p249). Thus, monthly retrievals where LAI $\geq$1.5 m^2 m^{-2} are considered high quality and we check the impact of quality (high/low) on our results. As described below, our spatial analysis focuses on the distribution of maximum growing season $V_{cmax}^{25,toc}$. This quantity can be determined for 90% of the vegetated global land-surface when implementing the aforementioned LAI $\geq$0.5 m^2 m^{-2} filter.

The PFT dependency of Eq. 2 requires knowledge of global land cover. Thus, the dominant landcover in each 0.5° grid cell is taken from the map of Goldwijk et al (2011) for the year 1990 and each cell assigned to one of the PFTs in Tab. 3. The adopted PFTs are based on the land-surface model JULES-SF (Alton 2016; Alton 2017, given that the long-term goal is to assimilate global $V_{cmax}^{25,toc}$ derived in this study into the carbon calculation of this model. Various sources for landcover are available (e.g. Loveland et al 2000;

Hansen & Reed 2000) but Goldwijk et al distinguishes carefully between natural and anthropogenic (pasture and cultivation) landcover, which could be important in terms of N-availability and biochemical change. To distinguish cells dominated by C_3 grasses/crops from those dominated by C_4 grasses/crops, we use the global map of Still et al (2003) which quantifies the fraction of C_4 vegetation in each grid-cell. Although each grid-cell is attributed to a single dominant PFT, the value of b_{wull} adopted in Eq. 2 differs greatly according to the photosynthetic pathway (§3.1). Therefore, the retrieval of $V_{cmax}^{25,toc}$ from the look-up table associated with Eq. 2 is conducted separately for the C_3 and C_4 fractions of each 0.5° cell. The final retrieved $V_{cmax}^{25,toc}$ for the grid-cell is the weighted mean of these two components. For dominant (assigned) PFTs with a C_3 pathway, the C_4 fraction is assumed to be C_4 grass, except for C_3 crop where C_4 crop is assumed for the C_4 fraction. For cells assigned as C_4 crop (C_4 grass), the C_3 fraction is assumed to be C_3 crop (C_3 grass).

The retrieved values of $V_{cmax}^{25,toc}$ are examined both spatially and temporally. For the spatial analysis, monthly retrievals for each 0.5° landpoint, where available, are pooled and the three highest values from each complete year (2003-2011) extracted. The pool of extracted values is median averaged to produce a maximum growing season photosynthetic capacity for each 0.5° location ($V_{cmax}^{25,toc}$(grow)). Median-, rather than mean-, averaging is adopted since measured plant parameters such as V_{cmax}^{25} often possess a skewed frequency distribution (Wright et al 2005; Kattge et al 2009; Alton 2017). The global distribution of $V_{cmax}^{25,toc}$(grow) is assessed in terms of latitude and dominant PFT. For the temporal analysis, we determine the decadal trend in both monthly $V_{cmax}^{25,toc}$ and monthly LAI to contrast the biochemical and structural change in vegetation. This analysis is organised by latitude (zones are affected differentially by environmental change) and by landcover (vegetation types respond differently to environmental change).

Given that our long-term goal is to provide spatially and temporally parameters for land-surface and carbon models, we make the global maps of $V_{cmax}^{25,toc}(grow)$ and the corresponding $J_{max}^{25,toc}(grow)$ available via the internet and ftp server. Similarly, monthly global 0.5° maps of $V_{cmax}^{25,toc}$, $J_{max}^{25,toc}$ and the corresponding LAI, are also provided (see Appendix B).

3.4 Sensitivity Analysis

Retrieval of $V_{cmax}^{25,toc}$ for FLUXNET sites (Alton 2017) revealed, via Monte Carlo uncertainty analysis, that systematic errors (owing to input LAI and parameterisation of the biochemical relations) dominate over random errors associated with the remotely sensed variables (LAI and MTCI). Such systematic errors are best investigated using a series of 3 sensitivity analysis experiments:

1. The conversion of MTCI to ground chlorophyll concentration is based on ground truthing over primarily grass and crops (Dash et al 2010). A ground calibration over a landscape dominated by non-tropical broadleaf forest (Vuolo et al 2012) yields a slightly different relation (a_{mtci}=0.469 and b_{mtci}=-0.484; c.f. Tab. 2). This alternative calibration is implemented to test sensitivity to the relation between MTCI and ground chlorophyll concentration.

2. Even though we have formulated the J_{max}^{25}-Chl relation as PFT-dependent, field-based data exhibit a large dispersion even for the same vegetation type (Fig. 3). Furthermore, the relation is unknown for C_4 grass and C_4 crops. The PFT-dependent relations we adopt in the retrieval are arguably sufficient for 0.5° grid cells, where the responses of individual species average out. However, we test general sensitivity to the J_{max}^{25}-Chl relation by treating all PFTs with the same relation and observing the impact on the results. Given that non-tropical broadleaf forest is best defined by observations in Fig. 1, we adopt this PFT for the "universal" relation. We eschew a sensitivity test of the relation $J_{cmax}^{25} - V_{cmax}^{25}$ (Tab. 2), which is conservative across PFTs (Wullschleger 1993; Kattge et al 2009; Walker et al 2014) compared to the J_{max}^{25}-Chl relation.

3. Sensitivity to input LAI is tested using a recalibration based on field measurements. Alton (2017) achieves this by extracting MODIS LAI for the 7×7 cells (49 km^2) surrounding well-studied FLUXNET locations and comparing against ground measurements in the FLUXNET ancillary database (Agarwal 2012). However, although the sample size is large (n=234), the single-point FLUXNET field measurements do not account for landscape heterogeneity across the MODIS footprint. Though the sample size is smaller (n=38), a more accurate recalibration is obtained by comparing MODIS LAI against the BELMANIP field sites (Garrigues et al 2008) for which satellite high resolution maps have been used to scale up multiple LAI sampling to the MODIS footprint. This elaborate approach produces a more linear relationship between MODIS LAI and site LAI (Fig. 4), which can then be used to recalibrate MODIS LAI so that it is consistent with ground measurements. Note that input MODIS LAI is recalibrated using this relationship for each monthly timestep.

4 Results & Discussion

4.1 Retrieved $V_{cmax}^{25,toc}(grow)$: Validation and Range

To examine the range (this section) and the global distribution (next section) of the retrieval, we focus on the maximum growing season photosynthetic capacity retrieved across the 10 yr MERIS period ($V_{cmax}^{25,toc}(grow)$). Monthly retrievals are examined in the temporal analysis below (§4.3).

Given the complexity and uncertainties of the current method, $V_{cmax}^{25,toc}(grow)$ retrieved for global land points shows fair agreement with field-based compilations of photosynthetic capacity for the upper canopy (Tab. 4). Thus, the Root Mean Square (RMS) difference between the retrieved median per PFT and the mean average of field compilations (columns 2 and 3 of Tab. 4) is 25 μmol m^{-2} s^{-1} (20 μmol m^{-2} s^{-1}, when omitting savanna for which the discrepancy is quite large). Retrievals are generally somewhat smaller than field values. Thus, mean averaging across all PFTs, where a comparison is possible, the retrieval median is 2/3 the field average (33 μmol m^{-2} s^{-1} and 53 μmol m^{-2} s^{-1}, respectively). Note that field values are also subject to considerable uncertainty and often contain location sampling biases (e.g. under-representation of Asia in Wright et al (2005)). Furthermore, the majority are *inferred* from $A - c_i$ curves, rather than measured directly (A is net leaf photosynthesis and c_i is intercellular CO_2 concentration). They also depend on both the precise formulation adopted for the Farquhar photosynthesis model, which relates V_{cmax}^{25} to A, and the conditions of measurement (e.g. correction for both plant water stress and sub-optimal leaf temperatures).

The retrieval possesses a narrower range than field-based compilations. However, the latter also show considerable disparities amongst themselves for the same PFT (Fig. 5). The dispersion and disparities that characterise field-based values might arise in part from methodological differences. For example, Wullschleger (1993) does not take explicit account of either the temperature nor the assimilation compensation point of the leaf in his adopted Farquhar model. In their method, Beerling & Quick (1995) use maximum leaf photosynthetic rate for individual PFTs and the long-term c_i inferred from the leaf isotope ratio δ^{13}C. For the retrieval, several aspects may explain the narrow range for each PFT. First, the 0.5° retrieval cells contain PFTs other than the dominant (ascribed) PFT and they average across many species even for the same PFT. This averaging tends to remove the extremes captured by field-based values. Second, the observed J_{max}^{25}-Chl relation differs for species of the same PFT (Fig. 3) and this dispersion is unaccounted for in our adopted PFT-dependent relation. Any future improvement would have to take account of accessory pigments and other non-chlorophyll molecules contributing to light-harvesting and the efficiency of electron transport (Evans 1989; Mauseth 1998; Gurevitch et al 2006). In this respect, optical and near-infrared hyperspectra may offer potential, owing to their apparent sensitivity to a range of leaf molecules and properties (Smith et al 2002; Serbin et al 2012).

Field-based values consistently reveal that C_3 crops have higher photosynthetic capacity than other PFTs

(Wullschleger 1993; Kattge et al 2009) and this is corroborated by our retrievals (Tab. 4). We retrieve lower $V_{cmax}^{25,toc}(grow)$ for C_4 crops compared to C_3 crops owing to the higher efficiency of the C_4 photosynthetic pathway. An alternative retrieval, based on total-to-active N ratio (Houborg et al (2013); Appendix A), yields medians of 72 and 37 μmol m^{-2} s^{-1}, respectively, for C_3 and C_4 crops. These values are within 9% of the corresponding medians in Tab. 4 (73 and 34 μmol m^{-2} s^{-1}, respectively).

4.2 Global Distribution of $V_{cmax}^{25,toc}(grow)$ and $J_{max}^{25,toc}(grow)$

Highest global values in $V_{cmax}^{25,toc}(grow)$ (55-60 μmol m^{-2} s^{-1}) and $J_{max}^{25,toc}(grow)$ (130-140 μmol m^{-2} s^{-1}) occur in the mid-northern and mid-southern zones i. e. latitude (lat) at $\pm 38^{\circ}$). This coincides with a preponderance of C_3 crops and C_3 grass, including pasture (Fig. 6). In particular, highest retrieved values are concentrated within the USA grain belt, European pasture/cropland, the Ukraine bread basket and the Indian sub-continent (Figs. 7 and 8). Crops and many grasslands are dominated by annuals which invest a large fraction of available N in the photosynthetic apparatus in order to maximize growth over a single year (Hikosaka 2004).

4.3 Trends in $V_{cmax}^{25,toc}$ and LAI

We follow previous authors in monitoring change by latitude (often considered a proxy for climate). However, we also analyse by PFT since biochemical change, like physiological response to CO_2 fertilisation (Norby et al 2005; Luo et al 2006), may vary according to vegetation type and growth form.

Timeseries and significant ($p<0.05$) trends for monthly $V_{cmax}^{25,toc}$ and LAI, averaging across different latitude zones, are depicted in Figs. 9 and 10. Apart from the mid-northern zone (lat=15-45°), $V_{cmax}^{25,toc}$ exhibits a decline between -3.0±0.5% per decade and -6.8±1.8% per decade (Tab. 5). LAI trends are positive in the northern (lat=45–90°) and mid-northern zones (+2.7±1.0% per decade and +1.5±0.5% per decade, respectively). However, for latitudes between -45° and -15° (mid-southern zone), there is a significant *decrease* (-2.8±0.7% per decade). In the northern zone, the trends are noisy owing to a reduced number of 0.5° cells for averaging. This reduction is due to incomplete satellite coverage at high latitudes and the removal of low LAI (background-dominated) cells from the retrieval. To first order, $V_{cmax}^{25} \sim$ MTCI/LAI. Therefore, in part, the more pronounced decrease in $V_{cmax}^{25,toc}$ in the northern zone may be attributable to the concommitant increase in LAI. However, a comparable decrease in the mid-southern zone is coincident with a decrease, rather than an increase, in LAI.

The change in $V_{cmax}^{25,toc}$ is more pronounced when analysed by PFT rather than by latitudinal zone (Fig. 11 and Tab. 6). Indeed, the strong and varied PFT-responses cancel to some extent when averaging over zones which comprise several vegetation types. The PFT-trend is also fairly consistent across zones (R^2=0.48; $p<0.01$; Fig. 12). Thus, it is vegetation type and not just latitude (and by implication climate) which determines the change in photosynthetic capacity. For LAI, the PFT-trend does not exhibit consistency between zones (Fig. 12). Note that the correlation for $V_{cmax}^{25,toc}$ in Fig. 12 depends strongly on the pronounced negative trends for C4 grass and non-tundra shrub. Therefore, this result should be viewed with caution.

Trends in $V_{cmax}^{25,toc}$ for mixed forest, non-tropical broadleaf forest and C_3 crops (Tab. 6) are not significantly different from zero (Tab. 6). The predominance of these PFTs in mid-northern latitudes explains the insignificant change in this zone, which contrasts with the decline in $V_{cmax}^{25,toc}$ in the remaining zones. Interestingly, positive and negative trends do not cluster according to growth form. Thus, while C_4 grass exhibits a substantial decline (-9.0±1.4% per decade), the decrease for C_3 grass is much less substantial (-2.4±0.7% per decade). Potentially, photosynthetic pathway may account for the different responses of C_3 and C_4 grasses. The C_3 pathway is more Rubisco-limited (Prentice et al 2000) and any decrease in V_{cmax}^{25} is likely to have

an adverse impact on primary productivity. However, the responses for the *tree* growth form, which are all C3 pathway, vary greatly too (e.g. compare needleleaf and non-tropical broadleaf in Tab. 6).

The (near-) zero $V_{cmax}^{25,toc}$ trends for a mixture of PFTs and growth forms in the mid-northern zone (mixed forest and C_3 crops) might best be explained by a regional influence such as N-deposition within the industrial countries of North America and Europe. However, this would not account for the consistency in PFT-trend between zones (Fig. 12). Focussing on anthropogenic PFTs, where N might be less limiting, C_3 crops have the highest positive trend amongst all the PFTs (0.7±0.6% per decade). However, the trend is significantly negative for C_4 crops (-2.4±0.7% per decade) and it lies in the middle of the distribution for PFT-trends (Tab. 6).

Results from FACE predict a small *decrease* in Rubisco-limited photosynthetic capacity owing to acclimation to rising [CO_2] (Ainsworth & Long 2005; Leakey et al 2009). The response is expected to depend on growth form or functional group, with trees being less affected (-6%) than grasses/crops (-17%). Indeed, our own results reveal a decrease in $V_{cmax}^{25,toc}$ but, as discussed above, the magnitude of the response does not group strongly according to life form.

For structural change, NDVI, rather than LAI, has been chiefly monitored in the past. However, we can make a valid comparison between the two quantities because both are based on broadband red and near-infrared reflectance. Indeed, LAI is often derived from NDVI assuming a non-linear (saturating) relationship (Los et al 2000). Analysing AVHRR satellite data for 1980s, Myneni et al (1997) measure a 13% increase per decade in NDVI seasonal amplitude for the northern zone and a 9% increase per decade for the mid-northern zone. The increase can best be explained by a larger seasonal amplitude in LAI (although a change in leaf biochemistry and pigment composition cannot be excluded). Combining both AVHRR and MODIS data for the period 1982-2011, Los (2013) confirms a steep increase for *global* NDVI for the 1980s but a levelling off from about 2000. Likewise, although Zhou et al (2001) detect an NDVI increase similar to Myneni et al for the 1980s, their AVHRR data reveal a flattening or even declining global trend for the 1990s. Analysis of *LAI*, from AVHRR, reveals a global trend (<1% per decade) over the baseline 1982-2009 (Zhu et al 2016), which is an order of magnitude smaller that that detected by Myneni et al for NDVI during the 1980s. This is partly due to a zero trend for 2001-2009. For the relatively late period of the current study (2002-2012), we record a zero (flat) trend in global LAI based on MODIS data (-0.2±0.4% per decade; Tab. 5).

Studies of AVHRR NDVI over multiple decades (e.g. 1982-2005) suggest large (50%) differences in *regional* trends according to continent or latitude (Zhou et al 2001; Zhang et al 2007). In some cases, even decreasing trends are apparent. Mao et al (2013) detect greater positive multidecadal LAI trends at high northern latitudes (+3.6% per decade) using both AVHRR and MODIS data over the period 1982-2009. They attribute this finding to asymmetric south-to-north land surface warming. This tendency is corroborated to some extent in the current study with the most positive LAI trend in the northern zone (Tab. 5).

Taking these results together, we cannot exclude the possibility of acclimation of LAI to environmental change or indeed a trend-reversal. Nevertheless, we are cautious about inferring long-term trends from the short (∼10 yr) timescales used in this study. Low frequency variations associated with natural climate oscillations (e.g. ENSO) or episodic volcanic aerosol may convolute long-term trends (Myneni et al 1997). For example, both $V_{cmax}^{25,toc}$ and LAI appear to undergo a ∼6 yr oscillation in Fig. 10 for the tropics (lat= -15° to 15°). Furthermore, part of the strongly negative trends for C4 grass and non-tundra shrub (-9.0±1.4% per decade and -13.1±1.6%, respectively) can be attributed to a pronounced decline in $V_{cmax}^{25,toc}$ at the end of the timeseries (2010-2012). This is also apparent in the mid-southern zone, where these PFTs contribute strongly to the land-cover (panel (b) of Fig. 10). A further consideration is that consistent sampling of LAI (and NDVI) across our satellite period (2002-2012) is rendered difficult by interannual variability in snow cover, sensitivity to soil background at the vegetation line and incomplete satellite coverage at lat>50°

during winter. Indeed, we believe that the purported increase in NDVI owing to earlier snowmelt (Myneni et al 1997), would be difficult to detect using remote sensing. Thicker snow cover in one year would actually bias measurements towards lower latitudes where mean LAI is higher. Our filter LAI<0.5 m^2m^{-2}, intended to reduce the influence of soil background, also precludes detection of a change at the northern boundary of vegetation cover.

What do field measurements reveal about LAI trend? Using the FLUXNET ancillary database (Agarwal 2012), for those few sites with regular long-term field measurements (approximately spanning 1997-2010), we obtain increases in LAI monthly anomaly for both non-tropical broadleaf trees (10±3.0% per decade) and needleleaf trees (4.0±2.5% per decade). Within Tab. 6, the latter agrees quite closely (2.4±1.5% per decade) but our increase for non-tropical broadleaf forest is an order of magnitude less (1.5±0.8% per decade). We note, however, that many FLUXNET sites are secondary and recovering from disturbance (Law et al 2002; Friend et al 2007). As such, they may represent rather poorly the average structural change across the 15-90° zone over which they are scattered.

4.4 Sensitivity Analysis & Limitations of Methodology

The following results follow from the sensitivity analysis:

1. Implementing alternative parameterisations for the biochemical relations, i.e. MTCI *versus* ground chlorophyll concentration (experiment 1) and J_{max}^{25}-*Chl* (experiment 2), produces no significant change in the main results. Thus, the inferred zonal trends in $V_{cmax}^{25,toc}$ and LAI change only modestly (±0.5% per decade) compared to uncertainties in the original trends (±0.8% per decade (RMS); Tab. 5). Furthermore, the PFT trends in $V_{cmax}^{25,toc}$ (Fig. 12) still correlate fairly well between zones (R^2=0.45-0.47 *versus* R^2=0.48 in the original retrieval; p<0.02).

2. Our results are more sensitive to the systematic (calibration) uncertainty in input LAI (experiment 3). Thus the RMS difference between the two retrievals of $V_{cmax}^{25,toc}(grow)$ (with and without recalibration to site LAI) is 7 μmol m^{-2} s^{-1}. However, this represents a moderate (20%) change (column 2 of Tab. 4). The impact is less than the RMS difference between the original (unrecalibrated) retrieval and the field average (25 μmol m^{-2} s^{-1}). The LAI recalibration also changes the inferred zonal trends for $V_{cmax}^{25,toc}$ and LAI by a moderate amount (0.8% per decade) compared to the original uncertainties (0.6-1.0% per decade). The decadal declines for zonal $V_{cmax}^{25,toc}$ remain statistically significant but the increases in LAI for the northern and mid-northern zones are somewhat reduced compared to the original retrieval (from 0.2-1.6% per decade to 1.5-2.7% per decade). With recalibration, the PFT trends in $V_{cmax}^{25,toc}$ still correlate to some extent between zones (R^2=0.46; p<0.02). We note that our inferred trends in both LAI and $V_{cmax}^{25,toc}$ depend on the accuracy and reliability of updates to the MODIS LAI product. Thus, the C6 release, adopted in the current study, corrects a long-term detector deterioration in the Terra instrument which spuriously generated negative LAI trends in previous releases (Yan et al 2016; Zhang et al 2017).

3. Our main results for LAI are robust when only accepting high quality retrievals which are less sensitive to soil background (i. e. LAI≥ 1.5 m^2m^{-2}; §3.3). However, zonal trends in $V_{cmax}^{25,toc}$ change more than the original uncertainties. This is because the temporal response of those PFTs comprising the zone varies according to LAI category. An extreme case is C3 grass within the mid-northern zone which possesses a decadal trend of -3.8±1.8% per decade for LAI< 1.5 m^2m^{-2} but +4.5±1.1% per decade for LAI≥ 1.5 m^2m^{-2}. The dichotomy stems from a substantial and non-spurious difference in decadal change of MTCI between both LAI categories. It does *not* arise from increased sensitivity to soil background, for which the uncertainty is much smaller than the decadal change in MTCI. In conclusion, our original results for $V_{cmax}^{25,toc}$ trend should be viewed with the caveat that temporal response varies greatly according to both PFT (Tab. 6) and canopy density (low and high LAI).

In summary of our sensitivity tests, the accuracy of the input satellite LAI ultimately limits the accuracy with which we can derive global $V_{cmax}^{25,toc}$ and determine the decadal trend in both LAI and $V_{cmax}^{25,toc}$. In comparison, incomplete empirical knowledge of biochemical relations (e.g. J_{max}^{25}-Chl) for some PFTs (e.g. C_4 grass) appears less problematic.

4.5 Environmental Change, Vegetation Productivity and the Carbon Cycle

Are the trends we infer for $V_{cmax}^{25,toc}$ and LAI important in the context of other environmental changes that can have an impact on carbon uptake? The IPCC (2013) identifies increasing [CO_2] as probably the most influential factor on vegetation productivity through CO_2 fertilisation. Indeed, numerous FACE experiments measure a $\simeq$30% increase in both diurnal and light-saturated carbon uptake when leaves are subjected to a 50% (160 ppm) increase in [CO_2]. For the observed rate of increasing [CO_2] (Keeling et al 1996), this corresponds to a 2-3% increase in productivity per decade. Increases in observed net primary productivity follow a similar trend, or about half ($\simeq$1% per decade) for non-woody vegetation (Norby et al 2005).

Climate-driven trends are more difficult to quantify. The C^4IMP modelling exercise predicts a -1.3$\pm$2.6% change in global net primary productivity per 1K rise in average air temperature, with models possessing varied responses to both increased temperature and reduced soil moisture availability (Friedlingstein et al 2006). For the observed rate of increasing temperature (Keeling et al 1996), this corresponds to a trend of -0.2$\pm$0.4% per decade in global net primary productivity. CMIP5 trends for the recent (satellite) period 1982-2011 yield -0.6$\pm$0.8% per decade (Smith et al 2016). Therefore, the trends we infer for zonal $V_{cmax}^{25,toc}$ are of a similar magnitude as those associated with CO_2 fertilisation and even larger than climate-related trends. However, we recognise that changes in $V_{cmax}^{25,toc}$ and gross productivity are unlikely to be proportional, given that photosynthesis is often constrained by factors other than Rubisco concentration (e.g. temperature and water).

As discussed above, FACE predicts a 6-17% *decrease* in V_{cmax}^{25} under rising [CO_2], equivalent to -1.0$\pm$0.5% per decade (Keeling et al 1996). Our derived PFT trends are up to an order of magnitude greater (Tab. 6). We speculate, therefore, that the expected long-term [CO_2] acclimation is masked by a shorter term response to other environmental factors, such as a multi-annual climate cycles (e.g. ENSO) or anthropogenic N emissions.

Structural change, such as LAI, may also have a non-proportional impact on gross productivity, although the 9-13% increase in NDVI, recorded by Myneni et al (1997) for the 1980s, is probably as least as important as CO_2 fertilisation over this period. The LAI decadal trends that we record for the mid-northern and northern zones (1.5-2.7% increase per decade; Tab. 5) are smaller in magnitude than the NDVI trend for the 1980s. This suggests that structural and biochemical trends may diminish (or even reverse) in time, perhaps owing to acclimation.

5 Summary and Conclusions

We employ a novel retrieval of top-of-canopy Rubisco-limited photosynthetic capacity (i.e. maximum carboxylation rate, $V_{cmax}^{25,toc}$) from remote sensing inputs of MODIS LAI and the MERIS terrestrial chlorophyll index (MTCI). Monthly values of $V_{cmax}^{25,toc}$ and light-limited photosynthetic capacity ($J_{max}^{25,toc}$) are retrieved for the period 2002-2012 for global 0.5° landpoints. The retrieved ranges of maximum growing season $V_{cmax}^{25,toc}$ are analysed spatially in terms of global PFTs and compared against compilations of field-based values. We examine the decadal trend in both $V_{cmax}^{25,toc}$ and LAI in order to ascertain biochemical and structural responses of vegetation to environmental change. The main conclusion is that both biochemical and structural trends are important, if sustained, when compared against other environmental factors which affect vegetation

productivity and carbon uptake (e.g. CO_2 fertilisation and climate).

Specific findings are as follows:

1. Highest global values in maximum growing season $V_{cmax}^{25,toc}$ (55-60 μmol m^{-2} s^{-1}) and $J_{max}^{25,toc}$ (130-140 μmol m^{-2} s^{-1}) occur in the mid-northern and mid-southern zones (lat=$\pm$38°), especially where C_3 crops dominate (i. e. the grain belts and breadbaskets of Europe, the USA, the Ukraine and India).

2. Analysed by PFT, the retrieved global values of maximum growing season Rubisco-limited photosynthetic capacity are somewhat lower, and possess a narrower range, than compilations of field-based values. Future improvement of the retrieval could take account of species differences in electron transport (e.g. accessory pigments) by assimilating hyperspectra or a greater number of narrow-band indices (Serbin et al 2015).

3. We detect a general temporal decline in $V_{cmax}^{25,toc}$ (between -0.3% per decade and -6.8% per decade, depending on latitude) for the period 2002-2012. However, the decadal trends for $V_{cmax}^{25,toc}$ depend more on PFT than latitude, suggesting that biochemical change, like physiological response (e.g. owing to CO_2 fertilisation; Norby et al 2005; Ainsworth & Long 2005), might best be monitored in terms of vegetation type rather than climate zone.

4. The greatest uncertainty in the retrieval stems from systematic errors in LAI but our main results appear to be robust even when recalibrating MODIS to upscaled ground measurements.

5. We record a zero (flat) trend in global LAI during 2002-2012 (-0.2$\pm$0.4% per decade). Furthermore, our LAI trends over this period for mid-northern (+1.5$\pm$0.5% per decade; lat=15-45°) and northern (+2.7$\pm$1.0% per decade; lat>45°) zones are much smaller than the substantial increases recorded in NDVI for the 1980s (9-13%; Myneni et al (1997)). Our results tentatively corroborate the finding that LAI trends are more positive towards higher northern latitudes (Mao et al 2013).

6 Appendix A: alternative retrieval of $V_{cmax}^{25,toc}$ for C_3 and C_4 crops based on Houborg et al (2013)

In their Tab.2, Houborg et al (2013) provide an empirical relation between leaf chlorophyll content (Chl; g m^{-2}) and the maximum carboxylation rate at 25°C (V_{cmax}^{25}; μmol m^{-2} s^{-1}) for C_3 and C_4 crops. This is based on the observed ratio between total and active leaf-N. Thus:

$$\frac{V_{cmax}^{25}(L) - b_{houb}}{a_{houb}} = Chl(L) \tag{6}$$

for a leaf located at a cumulative (i.e. from the canopy top) LAI equal to L. For C_3 leaves, the empirical constants a_{houb} and b_{houb} are 253 and -27, respectively. For C_4 leaves, a_{houb} and b_{houb} are 98.8 and -8.6, respectively.

Several authors measure an exponential decrease in active foliar N according to leaf position (expressed as cumulative LAI), such that:

$$V_{cmax}^{25}(L) = V_{cmax}^{25,toc} exp(-k_{rub} L) \tag{7}$$

where $V_{cmax}^{25,toc}$ is $V_{cmax}^{25}(L)$ at the canopy top and k_{rub} is the vertical N allocation parameter (Hirose & Werger 1987), for which we adopt an observationally based value of 0.15 (Carswell et al 2000; Lewis et al 2000; Meir et al 2002).

We substitute Eq. 7 into the left side of Eq. 6 and integrate both sides. Thus:

$$\int_0^{LAI} \frac{V_{cmax}^{25,toc} exp(-0.15L) - b_{houb}}{a_{houb}} \, dL = \int_0^{LAI} Chl(L) \, dL \tag{8}$$

Leaf chlorophyll content, summed over the LAI of the canopy, yields the chlorophyll concentration per unit ground which is detected by the hyperspectral satellite index MTCI. Thus:

$$\int_0^{LAI} Chl(L) \, dL = (0.758 \times MTCI) - 1.05 \tag{9}$$

based on the calibration of MTCI when ground sampling vegetation across the MERIS footprint (Dash et al 2010).

We substitute Eq. 9 into the right side of Eq. 8 and evaluate the integral on the left side. Rearranging, this yields:

$$V_{cmax}^{25,toc} = \frac{a_{houb}(0.114 \times MTCI - 0.158) + 0.15 b_{houb} LAI}{1 - exp(-0.15 LAI)} \tag{10}$$

where negative values of $V_{cmax}^{25,toc}$, occurring at low MTCI (<1.39), are set to zero.

7 Appendix B: photosynthetic capacity database

Global maximum growing season photosynthetic capacity and monthly global maps of both photosynthetic capacity and LAI are all available at 0.5° resolution via the internet address:

http://ggluck.swansea.ac.uk/ftp/apaul/vcmax

For bulk download, they can also be obtained via anonymous ftp as follows:

1. ftp ggluck.swansea.ac.uk (set both name and password to 'anonymous')
2. cd apaul/vcmax/global

Maximum growing season photosynthetic capacity is available in the file calc_vcmax_global_grow.out. Columns are as follows: (1)lat[°], (2)longitude[°], (3)$V_{cmax}^{25,toc}(grow)$ [μmol m^{-2} s^{-1}] and (4)$J_{max}^{25,toc}(grow)$ [μmol m^{-2} s^{-1}]. Monthly maps are available in subdirectories organised according to year. For example, maps for 2002 can be accessed via:

3. cd 2002
4. prompt
5. mget *
6. quit

Within each subdirectory, files are named calc_vcmax_global_<month>.out where <month> is between 1 and 12 for January to December. Columns are as follows: (1)lat[°], (2)longitude[°], (3)$V_{cmax}^{25,toc}$ [μmol m^{-2} s^{-1}], (4)$J_{max}^{25,toc}$ [μmol m^{-2} s^{-1}] and (5)LAI [m^{2}m^{-2}]. For both the monthly maps and the maximum growing season map, water bodies and unavailable land points are filled with values of -9999 and -999, respectively.

Acknowledgements

MTCI data are provided courtesy of the NERC Earth Observation Data Centre (NEODC) and ESA who provided the original data and Astrium GEO-Information Services who processed this data. We acknowledge the support of the TRY initiative on plant traits (http://www.try-db.org) which is maintained by J. Kattge and G. Boenisch at Max Planck Institute for Biogeochemistry, Jena, Germany. The leaf database of Walker et al (2014) was accessed via the Land Processes Distributed Active Archive Center (DAAC).

References

Agarwal, D., (ed.) 2012 Biological and Ancillary Data for FLUXNET sites. Data set. Available on-line [http://www.fluxdata.org]

Ainsworth, E., Long, S. (2005) What have we learned from 15 years of free-air CO_2 enrichment (FACE)? A meta-analytic review of the responses of photosynthesis, canopy properties and plant production to rising CO_2. New Phytol., 165(2):351-71.

Alton P. (2016) The sensitivity of models of gross primary productivity to meteorological and leaf area forcing: a comparison between a Penman-Monteith ecophysiogical approach and the MODIS Light-Use Efficiency algorithm *Agricultural and Forest Meteorology*, 218-219, 11-14

Alton, P., (2017) Retrieval of seasonal Rubisco-limited photosynthetic capacity at global FLUXNET sites from hyperspectral satellite remote sensing:Impact on carbon modelling *Agricultural and Forest Meteorology*, 232, 74-88

Beerling, D., Quick, W. (1995) A new technique for estimating rates of carboxylation and electron transport in leaves of C_3 plants for use in dynamic global vegetation models *Global Change Biology*, 1, 289-294

Bonan, G. B., P. J. Lawrence, K. W. Oleson, S. Levis, M. Jung, M. Reichstein, D. M. Lawrence, and S. C. Swenson (2011), Improving canopy processes in the Community Land Model version 4 (CLM4) using global flux fields empirically inferred from FLUXNET data, J. Geophys. Res., 116, G02014, doi:10.1029/2010JG001593.

Campbell, B. and Norman, J. (1998) Environmental Biophysics *Ed. Springer-Verlag, New York*

Carswell, F, Meir, P., Wandelli, E. et al (2000) Photosynthetic capacity in a central Amazonian rain forest *Tree Physiology* 20, 179-186

Clark, R.N., G.A. Swayze, A. Gallagher, T.V.V. King, and W.M. Calvin, (1993), The U. S. Geological Survey, Digital Spectral Library: Version 1: 0.2 to 3.0 um, U.S. Geological Survey, Open File Report 93-592, 1326 pages.

Cleveland, C., Houlton, B., Smith, W., Marklein, A., Reed. S., Parton, W., del Grosso, S., Running, S., (2013) Patterns of new versus recycled primary production in the terrestrial biosphere, *PNAS*, 110, 12733-12737

Collatz, G., Ball, J., Grivet, C., Berry, J. (1991) Physiological and environmental regulation of stomatal conductance, photosynthesis and transpiration: a model that includes laminar boundary layer *Agric.For.Meteorol.* 54, 107-136

Collatz, G., Ribas-Carbo, M., Berry, J., (1992) Coupled photosynthesis-stomatal conductance model for leaves of C_4 plants *Aust. J. Plant Physiol.*, 19, 519-538

Curran, P, Dash, J., Lankester, T., Hubbard, S., (2007) Global composites of the MERIS Terrestrial Chlorophyll Index *Int.Journal of Remote Sensing*, 28, 3757-3758

Dang, Q., Margolis, H., and Collatz, G. (1998) Parameterization and testing of a coupled photosynthesis-stomatal conductance model for boreal trees *Tree Physiology, 18*, 141-153

Dash, J., Curran, P. (2007) Evaluation of the MERIS chlorophyll index (MTCI) *Advances in Space Research*, 39, 100-104

Dash, J., Curran, P.J., Tallis, M.J., Llewelyn, M., Taylor, Gail and Snoeij, P. (2010) Validating the MERIS Terrestrial Chlorophyll Index (MTCI) with ground chlorophyll content data at MERIS spatial resolution *Journal of Remote Sensing*, 31, (20), 5513-5532

De Kauwe, M.G.; Disney, M.I.; Quaife, T.; Lewis, P.; Williams, M. (2011) An assessment of the MODIS collection 5 leaf area index product for a region of mixed coniferous forest *Remote Sensing of Environment*, 115, 767-780

Evans, J. R. (1989) Photosynthesis and nitrogen relationships in leaves of C_3 plants. *Oecologia*, 78, 9-19

Fang, H., Wei, S., Liang, S. (2012) Validation of MODIS and CYCLOPES LAI products using global field measurements data *Remote Sensing of Environment*, 119, 43-54

Farquhar, G., von Caemmerer, S., Berry, J. (1980) A biochemical model of photosynthetic CO_2 assimilation in leaves of C_3 species *Planta*, 149, 78-90

Forkel, M., Carvalhais, N., Roedenbeck, C., Keeling, R., Heimann, M., Thonicke, K., Zaehle, S., Reichstein, M., (2016) Enhanced seasonal CO_2 exchange caused by amplified plant productivity in northern ecosystems *Science*, 351, 696-699

Friedlingstein, P., Cox, P, Betts, R, Bopp, L, von Bloh, W,Brovkin, V., Cadule, P., Doney, S., Eby, M., Fung, I., Bala, G., John, J., Jones, C., Joos, F., Kato, T., Kawamiya, M., Knorr, W., Lindsay, K., Matthews, H.D., Raddatz, T., Rayner, P, Reick, C., Roeckner, E., Schnitzler, K.-G., Schnur, R., Strassmann, K., Weaver, A.J., Yoshikawa, C., Zeng, N. (2006) Climate-carbon cycle feedback analysis: Results from the C4MIP model intercomparison *Journal of Climate*, 19, 3337-3353

Friend, A., Arneth, A., Kiang, N., Lomas, M., Ogee, J., Roedenbeck, C., Running, S., Santaren, J., Sitch, S., Viovy, N., Woodward, I., Zaehle, S., (2007) FLUXNET and modelling the global carbon cycle *Global Change Biology*, 13, 610-633

Garrigues, S., Lacaze, R., Baret, F., Morisette, J., Weiss, M., Nickeson, J., Fernandes, R., Plummer, S., Shabanov, N., Myneni, R., Knyazikhin, Y., Yang, W., (2008) Validation and intercomparison of global leaf area index products derived from remote sensing *Journal of Geophysical Research*, 113, G02028

Goldwijk, K., Beusen, A., van Drecht, G., de Vos, M., (2011) The HYDE 3.1 spatially explicit database of human-induced global land-use change over the past 12,000 years *Global Ecology and Biogeography*, 20, 73-86

Grace ,J., Nichol, C., Disney, M, Lewis, P, Quaife, T., Bowyer, P.(2007) Can we measure terrestrial photosynthesis from space directly, using spectral reflectance and fluorescence? *Global Change Biology*, 13, 1484-1497

Graven, H., Keeling, R., Piper, S., Patra, P., Stephens, B., Wofsy, S., Welp, L., Sweeney, C., Tans, P., Kelley, J., Daube, B., Kort, E., Santoni, G., Bent, J., (2013) Enhanced seasonal exchange of CO_2 by northern ecosystems since 1960 *Science*, 341, 1085-1089

Guanter, L., Zhang, Y., Jung, M., Joiner, J., Voigt, M,. Berry, J., Frankenberg, C., Huete, A., Zarco-Tejada, P., Jung-Eun, L., Moran, M., Ponce-Campos, G., Beer, C., Camps-Valls, G., Buchmann, N. Gianelle, D.,

692 Klumpp, K., Cescatti, A., Baker, J., Griffis, T., Global and time-resolved monitoring of crop photosynthesis
693 with chlorophyll fluorescence (2014) *PNAS*, 111(14), E1327-E1333
694
695 Gurevitch, J., Scheiner, S., Fox, G., (2006) The Ecology of Plants, *Ed. Sinauer Associates, Sunderland, USA*
696
697 Hansen, M., Reed, B., (2000) A comparison of the IGBP DISCover and University of Maryland 1 km global
698 land cover products *Int. J. Remote Sensing*, 21, 1365-1373
699
700 Hikosaka, K. (2004) Interspecific difference in the photosynthesis-nitrogen relationship: patterns, physiolog-
701 ical causes, and ecological importance. *J.Plant Res.*,117, 481-494
702
703 Hirose, T., Werger, M. (1987) Maximising daily canopy photosynthesis with respect to leaf-N allocation
704 pattern in the canopy *Oecologia*, 72, 520-526
705
706 Houborg, R., Cescatti, A., Migliavacca, M., Kustas, W., (2013) Satellite retrievals of leaf chlorophyll and
707 photosynthetic capacity for improved modelling of GPP *Agricultural and Forest Meteorology*, 177, 10-23
708
709 Jones, H (1992) Plants and Microclimate, Cambridge University Press
710
711 IPCC (2013) Climate change 2013: the physical science basis. In Contribution of Working Group I to the
712 Fifth Assessment Report of the Intergovernmental Panel on Climate Change, Eds. Stocker TF, Qin D, Plat-
713 tner GK, Tignor M, Allen SK, Boschung J, Nauels A, Xia Y, Bex V, Midgley PM, Cambridge University
714 Press, Cambridge (UK) and New York, NY, (USA).
715
716 Kattge, J., Knorr, W., Raddatz, T., Wirth, C. (2009) Quantifying photosynthetic capacity and its relation-
717 ship to leaf-Nitrogen content for global-scale terrestrial biosphere models *Global Change Biology*, 15, 976-991
718
719 Keeling, C., Chin, J., Whorf, T., (1996) Increased activity of northern vegetation inferred from atmospheric
720 CO_2 measurements *Nature*, 382, 146-149
721
722 Law, B., Falge, E., Gu, L., D. D. Baldocchi, P. Bakwin, P. Berbigier, K. Davis, A. J. Dolman, M. Falk, J. D.
723 Fuentes, A. Goldstein, A. Granier, A. Grelle, D. Hollinger, I. A. Janssens, P. Jarvis, N. O. Jensen, G. Katul,
724 Y. Mahli, G. Matteucci, T. Meyers, R. Monson, W. Munger, W. Oechel, R. Olson, K. Pilegaard, K. T.
725 Paw U, H. Thorgeirsson, R. Valentini, S. Verma, T. Vesalaa, K. Wilson and S.Wofsy (2002) Environmental
726 controls over carbon dioxide and water vapour exchange of terrestrial vegetation *Agricultural and Forest*
727 *Meteorology*, 113, 97-120
728
729 Leakey, A., Ainsworth, E., Bernacchi, C., Rogers, A., Long, S., Ort, D., Elevated CO_2 effects on plant car-
730 bon, nitrogen, and water relations: six important lessons from FACE (2009) *J Exp Bot*, 60 (10): 2859-2876
731
732 Lewis, J., McKane, R., Tingey, D., Beedlow, P. (2000) Vertical gradients in photosynthetic light response
733 within an old-growth douglas-fir and western hemlock canopy *Tree Physiology* 20, 447
734
735 Los, S., Collatz, G., Sellers P., Malmstrom, C., Pollack, N., de Fries, R., Bounana, L., Parris, M., Tucker,
736 C., Dazlich, D., (2000) A global 9-yr biophysical land surface dataset from NOAA AVHRR data *Journal of*
737 *Hydrometeorology* 1, 183-199
738
739 Los, S., (2013) Analysis of trends in fused AVHRR and MODIS NDVI data for 1982-2006: indication for a
740 CO_2 fertilisation effect in global vegetation *Global Biogeochemical Cycles*, 27, 318-330
741

Lloyd, J., (1999) The CO_2 dependence of photosynthesis, plant growth responses to elevated CO_2 concentrations and their interaction with soil nutrient status, II. Temperate and boreal forest productivity and the combined effects of increasing CO_2 concentrations and increased nitrogen deposition at a global scale *Functional Ecology*, 13, 439-459

Loveland, T.R., Reed, B.C., Brown, J.F., Ohlen, D.O., Zhu, Z., Yang, L. & Merchant, J.W. (2000) Development of a global land cover characteristics database and IGBP DISCover from 1 km AVHRR data. International Journal of Remote Sensing, 21, 1303-1330

Luo, Y., Field, C., Jackson, R. (2006) Does nitrogen constrain carbon cycling, or does carbon input stimulate nitrogen cycling? *Ecology*, 87, 3-4

Mao, J., Shi, X., Thornton, P., Hoffman, F., Zhu, Z., Myneni, R. (2013) Global latitudinal-asymmetric vegetation growth trends and their driving mechanisms: 1982-2009

Mauseth, J. (1998), Botany: an introduction to plant biology, *Ed. Jones and Bartlett Publishers, Sudbury, USA*

Meir, P., Kruijt, B., Broadmeadow, M., Kull, O., Carswell, F., Nobre, A. (2002) Acclimation of photosynthetic capacity to irradiance in tree canopies in relation to leaf-N concentration and leaf mass per unit area *Plant, Cell and Environment* 25, 343-357

Middleton, E.M. McMurtrey, J.E. Entcheva Campbell, P.K. Butcher, L.M. Chappelle, E.W. (2003) Foliar Reflectance and Fluorescence Responses for Plants under Nitrogen Stress Determined with Active and Passive Systems, *International Geoscience and Remote Sensing Symposium (IGARSS).*

Myneni, R., Keeling, C., Tucker, C., Asrar, G., Nemani, R., (1997) Increased plant growth in the northern high latitudes from 1981 to 1991 *Nature*, 386, 698-702

Nadelhoffer, K., Emmett, B., Gundersen, P., Janne Kjonaas, O., Koopmans, C., Schleppi, P., Tietema, A., Wright, R., (1999) Nitrogen deposition makes a minor contribution to carbon sequestration in temperate forests *Nature*, 398, 145-148

Norby, R., Warren, J., Iversen, C., Medlyn, B., McMurtrie, R. (2005) CO_2 enhancement of forest productivity constrained by limited nitrogen availability *PNAS*, 107, 19368-19373, 2010

Ollinger, S. V., Reich, P. B., Frolking, S., Lepine, L. C., Hollinger, D. Y., & Richardson, A. D., (2013), Nitrogen cycling, forest canopy reflectance, and emergent properties of ecosystems. *Proc Natl Acad Sci.*, 110(27), E2437

Peng, Y., Nguy-Robertson, A., Arkebauer, T., Gitelson, A., (2017) Assessment of canopy chlorophyll content retrieval in maize and soybean: implications of hysteresis on the development of generic algorithms *Remote Sensing*, 9, 226

Prentice, I., Heimann, M., Sitch, S., (2000) The carbon balance of the terrestrial biosphere: ecosystem models and atmospheric observations *Ecological Applications*, 10(6), 1553-1573

Rogers A (2014) The use and misuse of Vcmax in Earth System Models. *Photosynthesis Research* 119, 15-29

Ryu, Y., Baldocchi, D., Kobayashi, H., van Inge, C., Lie, J. (2011) Integration of MODIS land and atmo-

sphere products with a coupled-process model to estimate gross primary productivity and evapotranspiration from 1 km to global scales *Global Biogeochemical Cycles* 25(4), GB4017

Sage, R., Pearcy, R., Seeman, J. (1987) The nitrogen use efficiency of C_3 and C_4 plants *Plant Physiology*, 85, 355-359

Sellers, P., Randall, D., Collatz, G., et al (1996) A revised land surface parameterization (SiB2) for atmospheric GCMs. Part I: Model formulation *Journal of Climate* 9, 676-705

Serbin, S, Dillaway D, Kruger, E, Townsend, P. (2012) Leaf optical properties reflect variation in photosynthetic metabolism and its sensitivity to temperature *J.Experimental Botany*, 63, 489-502

Serbin, S., Ahl, D., Stith, G. (2013) Spatial and temporal validation of the MODIS LAI and FPAR products across a boreal forest wildfire chronosequence *Remote Sensing of Environment*, 133, 71-84

Serbin, S., Singh, A., Desai, A., Dubois, S., Jablonski, A., Kingdon, C., Kruger, E., Townsend, P., (2015) Remotely estimating photosynthetic capacity, and its response to temperature, in vegetation canopies using imaging spectroscopy *Remote Sensing of Environment*, 167, 78-87

Shabanov, N., Huang,D., Yang W., Tan B., Knyazikhin Y., Myneni R., Ahl D. , Gower S, Huete A. , Arago L-E, Shimabukuro, Y., (2005) Analysis and optimization of the MODIS Leaf Area Index algorithm retrievals over broadleaf forests

Smith, M-L, Ollinger, S., Martin, M., Aber, J., Hallett, R., Goodale, C., (2002) Direct estimation of aboveground forest productivity through hyperspectral remote sensing of canopy nitrogen *Ecological Applications*, 12(5), 1286-1302

Smith, B., Warlind, D., Arneth, A., Hickler, T., Leadley, P., Siltberg, J., Zaehle, S., (2014) Implications of incorporating N cycling and N limitations on primary production in an individual-based dynamic vegetation model *Biogeosciences*, 11, 2027-2054

Smith, W., Reed, S., Cleveland, C., Ballantyne, A., Anderegg, W., Wieder, W., Liu, Y., Running, S., (2016) Large divergence of satellite and earth system model estimates of global terrestrial CO_2 fertilisation *Nature Climate Change*, 6, 306-310

Still, C. J., J. A. Berry, G. J. Collatz, and R. S. DeFries (2003), Global distribution of C_3 and C_4 vegetation: Carbon cycle implications, *Global Biogeochem. Cycles*, 17(1), 1006, doi:10.1029/2001GB001807

Townsend, A., Braswell, B., Holland, E., Penner. J., (1996) Spatial and temporal patterns in terrestrial carbon storage due to deposition of fossil fuel nitrogen *Ecological Applications*, 6(3), 806-814

Urbanski, S., Barford, C., Wofsy, S., Kucharik, C., Pyle, E., Budney, J., McKain, K., Fitzjarrald, D., Czikowsky, M., Munger, J., (2007) Factors controlling CO_2 exchange on timescales from hourly to decadal at Harvard Forest *JGR*, 112, G02020

Vuolo, F., Dash, J., Curran, P., Lajas, D., Kwiatkowska, E., (2012) Methodologies and uncertainties in the use of the Terrestrial Chlorophyll Index for the Sentinel-3 mission, *Remote Sensing*, 4, 1112-1133

Walker, A.P. Beckerman, L. Gu, J. Kattge, L.A. Cernusak, T.F. Domingues, J.C. Scales, G. Wohlfahrt, S.D. Wullschleger, F.I. Woodward (2014) The relationship of leaf photosynthetic traits to leaf-Nitrogen, leaf

phosphorus, and specific leaf area: a meta-analysis and modeling study *Ecol. Evol.*, 4, 3227-3235

Wong, S., Cowan, I., Farquhar, G. (1979) Stomatal conductance correlates with photosynthetic capacity *Nature*, 282, 424-426

Wright, I., Reich PB, Cornelissen JH, Falster DS, Garnier E, Hikosaka K, Lamont BB, Lee W, Oleksyn J, Osada N, Poorter H, Villar R, Warton DI, Westoby M. (2005) *New Phytol.*166(2):485-96

Wullschleger, S. (1993) Biochemical Limitations to Carbon Assimilation in C_3 Plants – A Retrospective Analysis of the A/Ci Curves from 109 Species *J.Expt.Biology*,44,907-920

Yan, K., Park., T., Yan, G., Liu, A., Yang, B., Chen, C., Nemani, R., Knyazikhin, Y., Myneni, R. (2016) Evaluation of MODIS LAI/FPAR Product Collection 6. Part 2: validation and intercomparison *Remote Sensing*, 8, 460-485

Yang, W, Shabanov, NV, Huang, D, Wang, W, Dickinson, RE, Nemani, RR, Knyazikhin, Y, Myneni, RB (2006). Analysis of leaf area index products from combination of MODIS Terra and Aqua data. *Remote Sensing of Environment*, 104(3), 297-312

Zaehle, S., Friend, A., Friedlingstein, P., Dentener, F., Peylin, P., Schulz, M., (2010) Carbon and nitrogen cycle dynamics in the O-CN land surface model: 2 role of the nitrogen cycle in the historical terrestrial carbon balance *Global Biogeochemical Cycles*, 24, GB1006

Zhao, M., Heinsch, F., Nemani, R., Running, S., (2005) Improvements of the MODIS terrestrial gross and net primary production global data set *Remote Sensing of Environment*, 95, 164-176

Zhang, X., Tarpley, D., Sullivan, J., (2007) Diverse responses of vegetation phenology to a warming climate *Geophysical Research Letters*, 34, L19405

Zhang, Y., Guanter, L., Berry, J.A., Joiner, J., van der Tol, C., Huete, A., et al. (2014). Estimation of vegetation photosynthetic capacity from space-based measurements of chlorophyll fluorescence for terrestrial biosphere models. Global Change Biology, 20,3727-3742

Zhang, Y., Conghe, S., Band., L., Sun, G., Li, J. (2017) Reanalysis of global terrestrial vegetation trends from MODIS products: browning or greening? *Remote Sensing of Environment*, 191, 145-155

Zhou, L., Tucker, C., Kaufmann, R., Slayback, D., Shabanov, N., Myneni, R. (2001) Variations in northern vegetation activity inferred from satellite data of vegetation index during 1981 to 1999 *Journal of Geophysical Research*, 106, 20069-20083

Zhu, Z., Shilong Piao, Ranga B. Myneni, Mengtian Huang, Zhenzhong Zeng, Josep G. Canadell, Philippe Ciais, Stephen Sitch, Pierre Friedlingstein, Almut Arneth, Chunxiang Cao, Lei Cheng, Etsushi Kato, Charles Koven, Yue Li, Xu Lian, Yongwen Liu, Ronggao Liu, Jiafu Mao, Yaozhong Pan, Shushi Peng, Josep Peuelas, Benjamin Poulter, Thomas A. M. Pugh, Benjamin D. Stocker, Nicolas Viovy, Xuhui Wang, Yingping Wang, Zhiqiang Xiao, Hui Yang, Soenke Zaehle, Ning Zeng (2016) Greening of the Earth and its drivers *Nature Climate Change*, 6, 791-795

Table 1: An alphabetical list of acronyms, abbreviations and quantities used frequently in the main text. Units are given where appropriate.

	Definition
Chl	Leaf chlorophyll content (g m^{-2})
$[CO_2]$	Atmospheric CO_2 concentration (ppm)
FACE	Free-air CO_2 enrichment
J_{max}	Maximum electron transport rate (μmol m^{-2} s^{-1}) (light-limited photosynthetic capacity)
J_{max}^{25}	J_{max} at 25°C (μmol m^{-2} s^{-1})
$J_{cmax}^{25,toc}$	J_{cmax}^{25} at canopy top (μmol m^{-2} s^{-1})
LAI	Leaf Area Index (m^2 m^{-2})
lat	latitude (°)
MERIS	MEdium Resolution Imaging Spectrometer
MODIS	Moderate Resolution Imaging Spectroradiometer
MTCI	MERIS Terrestrial Chlorophyll Index
N	Nitrogen
NDVI	Normalised Difference Vegetation Index
PFT	Plant Functional Type
RMS	Root Mean Square
V_{cmax}	Maximum carboxylation rate (μmol m^{-2} s^{-1}) (Rubisco-limited photosynthetic capacity)
V_{cmax}^{25}	V_{cmax} at 25°C (μmol m^{-2} s^{-1})
$V_{cmax}^{25,toc}$	V_{cmax}^{25} at canopy top (μmol m^{-2} s^{-1})

Table 2: Main steps and equations associated with the conceptual methodology. The corresponding step is enumerated and explained at the beginning of §3.1. Definition of the quantities and assignment of the best-fit coefficients are discussed in the main text. Note that b_{wull} differs according to the C_3 or C_4 photosynthetic pathway.

Step	Equation	Best-fit Coefficients
1	$J_{max}^{25}(L) = a_{chl} \times Chl(L) + b_{chl}$	PFT-dependent a_{chl} & b_{chl} (see text)
2	$\int_0^{LAI} Chl(L)dL = a_{mtci} \times MTCI + b_{mtci}$	a_{mtci}=0.616 g m^{-2}; b_{mtci}=-0.700 g m^{-2}
3	$J_{max}^{25}(L) = a_{wull}(1 - exp(-V_{cmax}^{25}(L)/b_{wull}))$	a_{wull}=428 μmol m^{-2} s^{-1} (C_3 & C_4); b_{wull}=158 μmol m^{-2} s^{-1} (C_3) b_{wull}=44 μmol m^{-2} s^{-1} (C_4)
4	$V_{cmax}^{25}(L) = V_{cmax}^{25,toc} exp(-k_{rub}L)$	k_{rub}=0.15

Table 3: Optimised coefficients for a_{chl} and b_{chl}, which relate J^{25}_{max} to leaf chlorophyll content (Chl; step 1 of T
Functional Type (PFT). PFT-design. is the abbreviated designation adopted for PFTs in subsequent tables and fig
is conducted separately for $Chl \leq 0.4$ g m^{-2} and for $Chl > 0.4$ g m^{-2} by varying a_{chl}. For $Chl \leq 0.4$ g m^{-2}, b_{chl}
the origin. For $Chl > 0.4$ g m^{-2}, b_{chl} is already constrained by the condition that both best-fit lines meet at Ch
are, respectively, the standard error and the total number of data used to optimise the fit. For tundra shrub and
scarce or highly dispersive, we fit only for a_{chl} across the whole Chl range. For C_4 grass and C_4 crops (no data), v
as C_3 grass and C_3 crops, respectively. $J^{25}_{max} - Chl$ measurements are only available for "pure" leaf types rather t
types. Therefore, for savanna and mixed forest, we adopt the mean coefficients of, respectively, C_4 grass and non-tund
broadleaf forest and needleleaf forest.

PFT	PFT-design.	$Chl \leq 0.4$ g m^{-2}	$Chl > 0.4$ g m^{-2}		SE
		a_{chl} (μmol s^{-1} g^{-1})	a_{chl} (μmol s^{-1} g^{-1})	b_{chl} (μmol m^{-2} s^{-1})	(μmol m^{-2} s
Non-tropical Broadleaf Forest	BL	311	53	103	1.7
Needleleaf Forest	NL	289	72	87	5.8
C_3 crop	Cr3	449	0	180	8.3
C_4 crop	Cr4	449	0	180	8.3
Tundra Shrub	Tu	147	147	0	6.4
Mixed Forest	MX	300	62	95	3.7
Tropical Broadleaf Forest	TBL	267	0	107	3.0
C_3 grass	C3	243	243	0	6.8
C_4 grass	C4	243	243	0	6.8
Non-tundra Shrub	SH	202	314	-45	3.2
Savanna	SAV	222	278	-22	5.0

Table 4: The median of maximum growing season photosynthetic capacity ($V_{cmax}^{25,toc}(grow)$) retrieved for global land points compared to a field-based average of V_{cmax}^{25} (Rubisco-limited photosynthetic capacity measured in the upper canopy). The field-based average uses the compilations of Kattge et al (2009), Wright et al (2005), Wullschleger (1993) and Beerling & Quick (1995) and mean averages the central value (mean or median) given by each compilation for that Plant Functional Type (PFT). PFTs are abbreviated according to Tab. 3. SD(field) is the standard deviation of the field-based mean from the central value of each compilation. The retrieved median, after recalibration to site LAI, is given in parentheses and is discussed in §4.4.

PFT	Retrieved $V_{cmax}^{25,toc}(grow)$ median [μmol m^{-2} s^{-1}]	Field V_{cmax}^{25} mean [μmol m^{-2} s^{-1}]	SD(field) [μmol m^{-2} s^{-1}]
BL	54(59)	45	8
NL	24(32)	39	14
Cr3	73(82)	103	14
Cr4	34(36)	–	–
Tu	8(14)	33	11
MX	46(54)	50	–
TBL	30(28)	51	16
C3	38(49)	60	12
C4	15(19)	30	–
SH	26(33)	52	5
SAV	16(19)	66	–

Table 5: Decadal trend in monthly anomalies of $V_{cmax}^{25,toc}$ and LAI according to latitude zones. For each anomaly, the
and intercept (b) are shown for a linear fit across the MERIS period 2002-2012. The equivalent decadal trend and
as Δ and $d\Delta$, respectively. Where trends are significant ($p<0.05$), they are flagged by an asterisk. For all fits, the
given by R^2.

Zone	Latitudes	$V_{cmax}^{25,toc}$				LAI		
		a	b	$\Delta \pm d\Delta$	R^2	a	b	$\Delta \pm d\Delta$
	(°)	(μmol m^{-2} s^{-1} [yr]$^{-1}$)	(μmol m^{-2} s^{-1})	(%/decade)	(–)	(m^2 m^{-2} [yr]$^{-1}$)	(m^2 m^{-2})	(%/decade)
North	+45 – +90	-0.25782	517.53349	-6.8±1.8(*)	0.12	0.003194	-6.4111	2.7±1.0(*)
Mid-North	+15 – +45	-0.01319	26.46981	-0.3±0.8	0.00	0.002817	-5.6541	1.5±0.5(*)
Tropics	-15 – +15	-0.06655	133.58858	-3.0±0.5(*)	0.23	0.000468	-0.9398	0.1±0.3
Mid-South	-45 – -15	-0.14382	288.70834	-5.4±1.0(*)	0.21	-0.004960	9.9570	-2.8±0.7(*)
Global	-90 – +90	-0.10039	201.51710	-3.5±0.5(*)	0.33	-0.000571	1.1471	-0.2±0.4

Table 6: As Tab. 5 but according to Plant Functional Type (PFT). PFTs are abbreviated according to Tab. 3.

PFT	$V_{cmax}^{25,toc}$				LAI			
	a	b	$\Delta \pm d\Delta$	R^2	a	b	$\Delta \pm d\Delta$	R^2
(–)	(μmol m^{-2} s^{-1} [yr]$^{-1}$)	(μmol m^{-2} s^{-1})	(%/decade)	(–)	(m^2 m^{-2} [yr]$^{-1}$)	(m^2 m^{-2})	(%/decade)	(–)
BL	-0.07355	147.64468	-1.9±1.2	0.02	0.002962	-5.9465	1.5±0.8	0.03
NL	-0.35398	710.57144	-11.6±2.3(*)	0.18	0.002979	-5.9796	2.4±1.5	0.02
Cr3	0.04426	-88.84431	0.7±0.6	0.01	0.005337	-10.7132	3.1±0.8(*)	0.11
Cr4	-0.07038	141.27366	-2.4±0.7(*)	0.10	0.006775	-13.5997	3.4±0.6(*)	0.22
Tu	-0.14710	295.28796	-10.9±4.2(*)	0.06	0.001736	-3.4845	2.0±1.7	0.01
MX	-0.00828	16.61265	-0.2±0.9	0.00	0.005977	-11.9979	2.6±0.9(*)	0.07
TBL	-0.09307	186.81759	-3.7±0.5(*)	0.32	-0.001813	3.6397	-0.4±0.2	0.02
C3	-0.07668	153.93081	-2.4±0.7(*)	0.08	0.000910	-1.8267	0.5±0.5	0.01
C4	-0.11590	232.64553	-9.0±1.4(*)	0.27	-0.002165	4.3469	-1.5±0.7(*)	0.04
SH	-0.32235	647.06955	-13.1±1.6(*)	0.38	0.006663	-13.3750	5.6±1.1(*)	0.18
SAV	-0.05397	108.32904	-4.0±0.7(*)	0.21	0.002000	-4.0142	0.8±0.5	0.02

Figure Captions:

Fig.1: Measured maximum electron transport for the light reaction against leaf chlorophyll content (Chl), the latter inferred from measured leaf-N. Measurements from Walker et al (2014) are for a standard leaf temperature of 25° (J^{25}_{max}), whilst measurements from the TRY database (Kattge et al 2009) are for an unspecified temperature (J_{max}). The solid and dashed lines represent a least-square linear fit for, respectively, $Chl \leq 0.4$ g m^{-2} and $Chl > 0.4$ g m^{-2}. Fits and abbreviations for each PFT are given in Tab. 3.

Fig.2: Hyperspectral MERIS filters (doubled hashed area), used for the MTCI index, compared against the broadband MODIS filters used for LAI (single hashed area; Shabanov et al 2005). Both sets of filter are compared to the laboratory-based spectral reflectance of a maple leaf (Acer *sp.*; Clark et al 1993). The steep increase in reflectance between the optical and near infrared domains, known as the red-edge, arises from strong chlorophyll absorption at 690 nm and high reflectance by leaf mesophyll cells at 750 nm.

Fig.3: Measured maximum electron transport for the light reaction (J^{25}_{max}) against leaf chlorophyll content (Chl) for two species of non-tropical broadleaf forest. The corresponding fit for this PFT is superimposed (see panel (a) of Fig. 1). For 0.4≥Chl≥0.6, mean J^{25}_{max} is 185 μmol m^{-2} s^{-1} for Eucalyptus *globulus* and 97 μmol m^{-2} s^{-1} for Liquidambar *styraciflua* (Sweetgum) i.e. 43% above and 25% below, respectively, the general PFT relation (solid and dashed lines).

Fig.4: Leaf Area Index (LAI) measured by MODIS plotted against single-point field measurements (FLUXNET; lower panel) and against multiple scaled ground measurements (BELMANIP; upper panel). MODIS LAI corresponds to a 7 km × 7 km area coincident with the site and extracted for the date of the field measurement. In both panels, markers vary according to PFT (abbreviated according to Tab. 3). Least-square best fits are shown using the function σ=a(1-exp(-x/b)), where a=4.482, b=1.968 for FLUXNET (σ(flux)) and a=7.531, b=4.828 for BELMANIP (σ(bel)). The inverse of σ(bel) is used to recalibrate monthly MODIS LAI in a sensitivity test of input LAI on the $V^{25,toc}_{cmax}$ retrieval (§3.4). FLUXNET and BELMANIP ground measurements are taken, respectively, from Agarwal (2012) and Garrigues et al (2008).

Fig.5: Barcharts comparing the interquartile range of retrieved $V^{25,toc}_{cmax}(grow)$, designated as "retrieval" in the legend, with the corresponding field-based range for the upper canopy. The retrieval is for global land points whereas the field-based ranges are based on extensive compilations by Kattge et al (2009), Wright et al (2005) and Wullschleger (1993). Beerling & Quick (1995; BQ) is based on a single estimate per PFT. Values are grouped according to PFT. Note that the retrieved range for C_4 crops is shown with C_3 crops (no field measurements are available for C_4 crops).

Fig.6: Zonal profile of retrieved maximum growing season light-limited and Rubisco-limited photosynthetic capacity ($J^{25,toc}_{max}(grow)$ and $V^{25,toc}_{cmax}(grow)$, respectively; lower panel) compared against land cover (upper panel). Land cover is represented as the percentage of total vegetation at each latitude and is compressed to basic life-forms (tree, grass/crop and shrub) for clarity.

Fig.7: Maximum growing season photosynthetic capacity ($V^{25,toc}_{cmax}(grow)$; μmol m^{-2} s^{-1}) retrieved for 0.5° global grid-squares. Note that for locations of sparse vegetation (LAI<0.5 m^2 m^{-2}), a retrieval is not possible (black). This figure is reproduced in colour in the online version of this article.

Fig.8: Global PFTs based on Goldwijk et al (2011) with modification according to the distribution of C_4 vegetation (Still et al 2003). Grid-squares are at 0.5° resolution. Land without vegetation is black. This figure is reproduced in colour in the online version of this article.

Fig.9: Trend in monthly $V^{25,toc}_{cmax}$ (solid) and LAI (dashed) anomalies for the period 2002-2012 for the northern

(panel a) and mid-northern (panel b) latitudinal zones. Significant trends, where present, are fitted with a solid ($V_{cmax}^{25,toc}$) and a dashed (LAI) straight line (Tab. 5). Mean values averaged across the 2002-2012 period are shown as $< V_{cmax}^{25,toc} >$ and $< LAI >$. Note that LAI anomalies are in units of 0.1 m^2m^{-2} but $< LAI >$ is in units of m^2m^{-2}. The y-axis range (LAI) for the northern zone is twice that of the mid-northern zone.

Fig.10: As Fig. 9 but for the tropics (panel a) and for the mid-southern zone (panel b).

Fig.11: Decadal trends in monthly anomalies of $V_{cmax}^{25,toc}$ (squares with solid errorbars) and LAI (squares with dashed errorbars), shown separately according to global plant functional type. Plant functional types are abbreviated according to Tab. 3. Errorbars represent the standard error.

Fig.12: The decadal trend for the mid-northern (+15° to +45°) zone plotted against that for the combined tropics and mid-southern zone (-45° to +15°). The trend is defined for monthly anomalies in $V_{cmax}^{25,toc}$ (panel a) and LAI (panel b), expressed as a percentage of the mean value over the period 2002-2012. Each marker denotes a different plant functional type. Outliers are labelled using the abbreviations in Tab. 3. The y=x line and significant best fit ($V_{cmax}^{25,toc}$ only) are represented, respectively, by dashed and solid lines.

Figure 1: Measured maximum electron transport for the light reaction against leaf chlorophyll content (Chl), the latter inferred from measured leaf-N. Measurements from Walker et al (2014) are for a standard leaf temperature of 25° (J^{25}_{max}), whilst measurements from the TRY database (Kattge et al 2009) are for an unspecified temperature (J_{max}). The solid and dashed lines represent a least-square linear fit for, respectively, $Chl \leq 0.4$ g m^{-2} and $Chl > 0.4$ g m^{-2}. Fits and abbreviations for each PFT are given in Tab. 3.

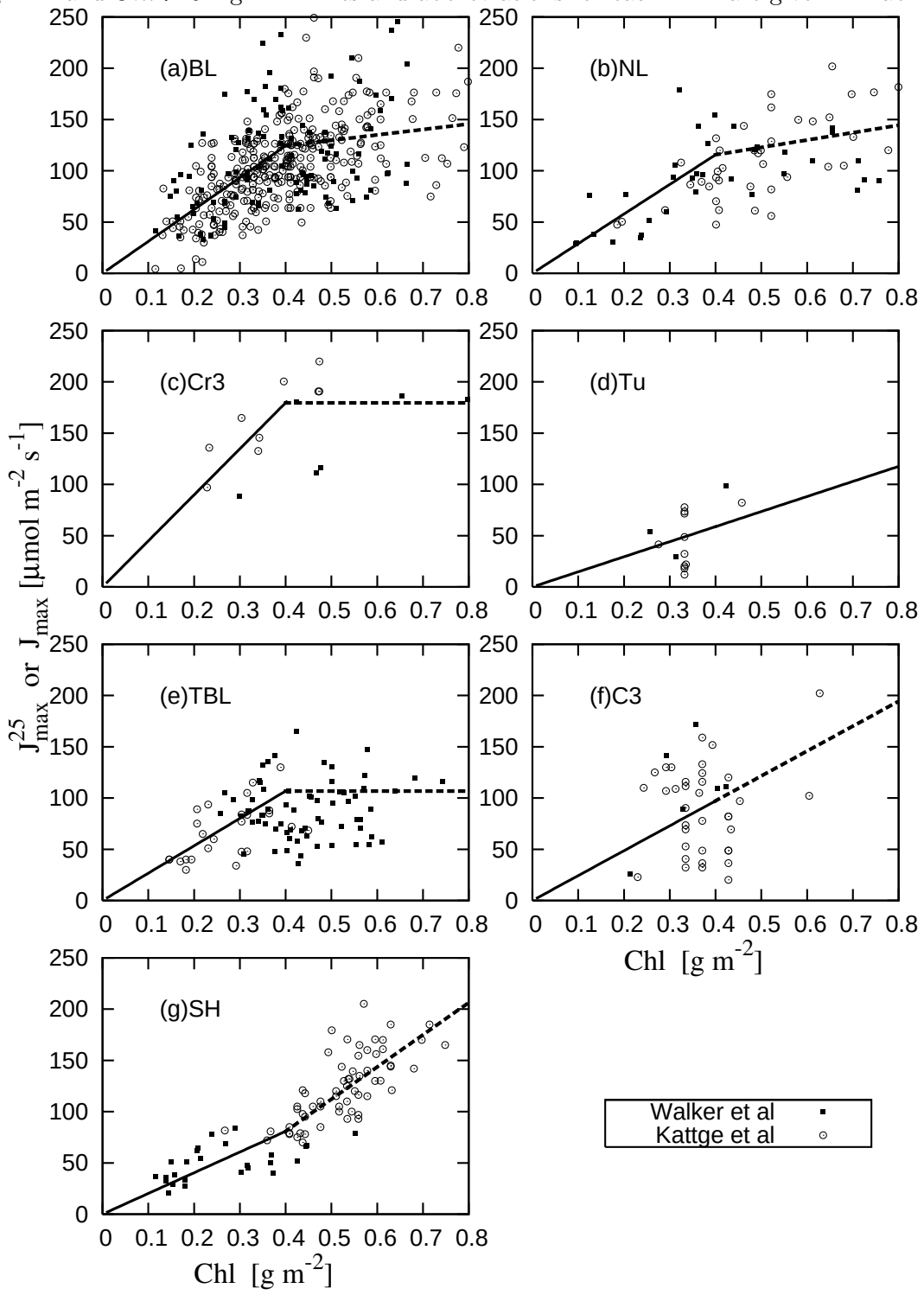

Figure 2: Hyperspectral MERIS filters (doubled hashed area), used for the MTCI index, compared against the broadband MODIS filters used for LAI (single hashed area; Shabanov et al 2005). Both sets of filter are compared to the laboratory-based spectral reflectance of a maple leaf (Acer *sp.*; Clark et al 1993). The steep increase in reflectance between the optical and near infrared domains, known as the red-edge, arises from strong chlorophyll absorption at 690 nm and high reflectance by leaf mesophyll cells at 750 nm.

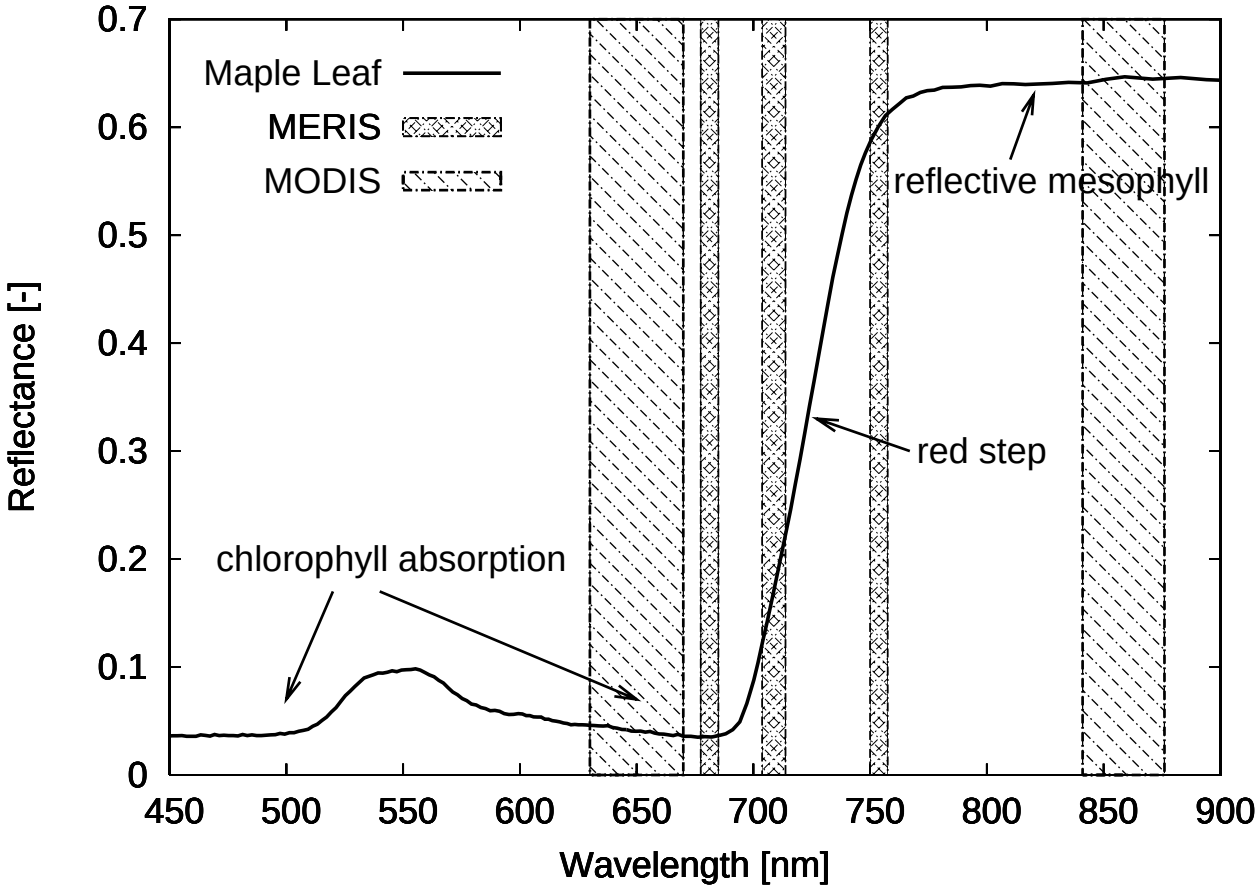

Figure 3: Measured maximum electron transport for the light reaction (J^{25}_{max}) against leaf chlorophyll content (Chl) for two species of non-tropical broadleaf forest. The corresponding fit for this PFT is superimposed (see panel (a) of Fig. 1). For 0.4≥Chl≥0.6, mean J^{25}_{max} is 185 μmol m^{-2} s^{-1} for Eucalyptus *globulus* and 97 μmol m^{-2} s^{-1} for Liquidambar *styraciflua* (Sweetgum) i.e. 43% above and 25% below, respectively, the general PFT relation (solid and dashed lines).

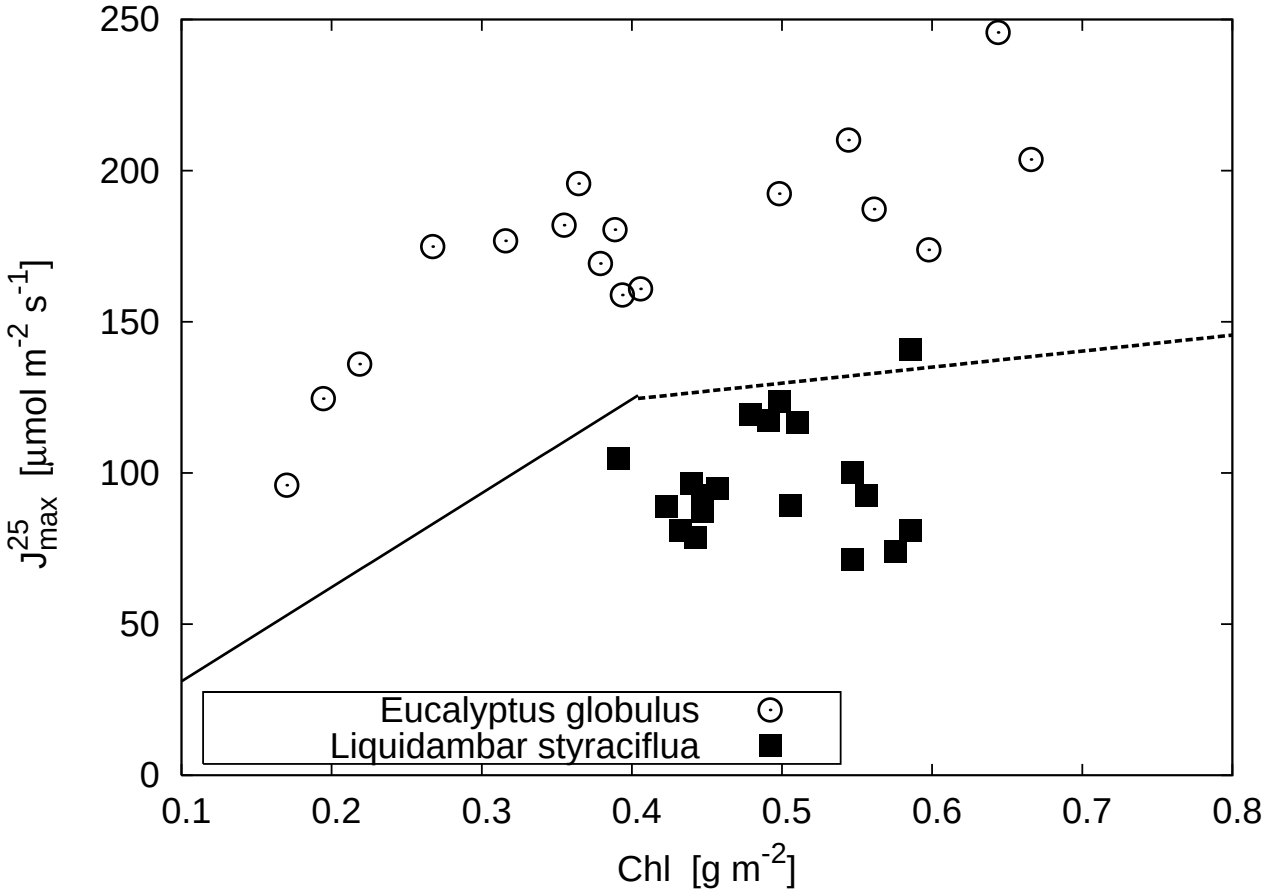

Figure 4: Leaf Area Index (LAI) measured by MODIS plotted against single-point field measurements (FLUXNET; lower panel) and against multiple scaled ground measurements (BELMANIP; upper panel). MODIS LAI corresponds to a 7 km × 7 km area coincident with the site and extracted for the date of the field measurement. In both panels, markers vary according to PFT (abbreviated according to Tab. 3). Least-square best fits are shown using the function σ=a(1-exp(-x/b)), where a=4.482, b=1.968 for FLUXNET (σ(flux)) and a=7.531, b=4.828 for BELMANIP (σ(bel)). The inverse of σ(bel) is used to recalibrate monthly MODIS LAI in a sensitivity test of input LAI on the $V_{cmax}^{25,toc}$ retrieval (§3.4). FLUXNET and BELMANIP ground measurements are taken, respectively, from Agarwal (2012) and Garrigues et al (2008).

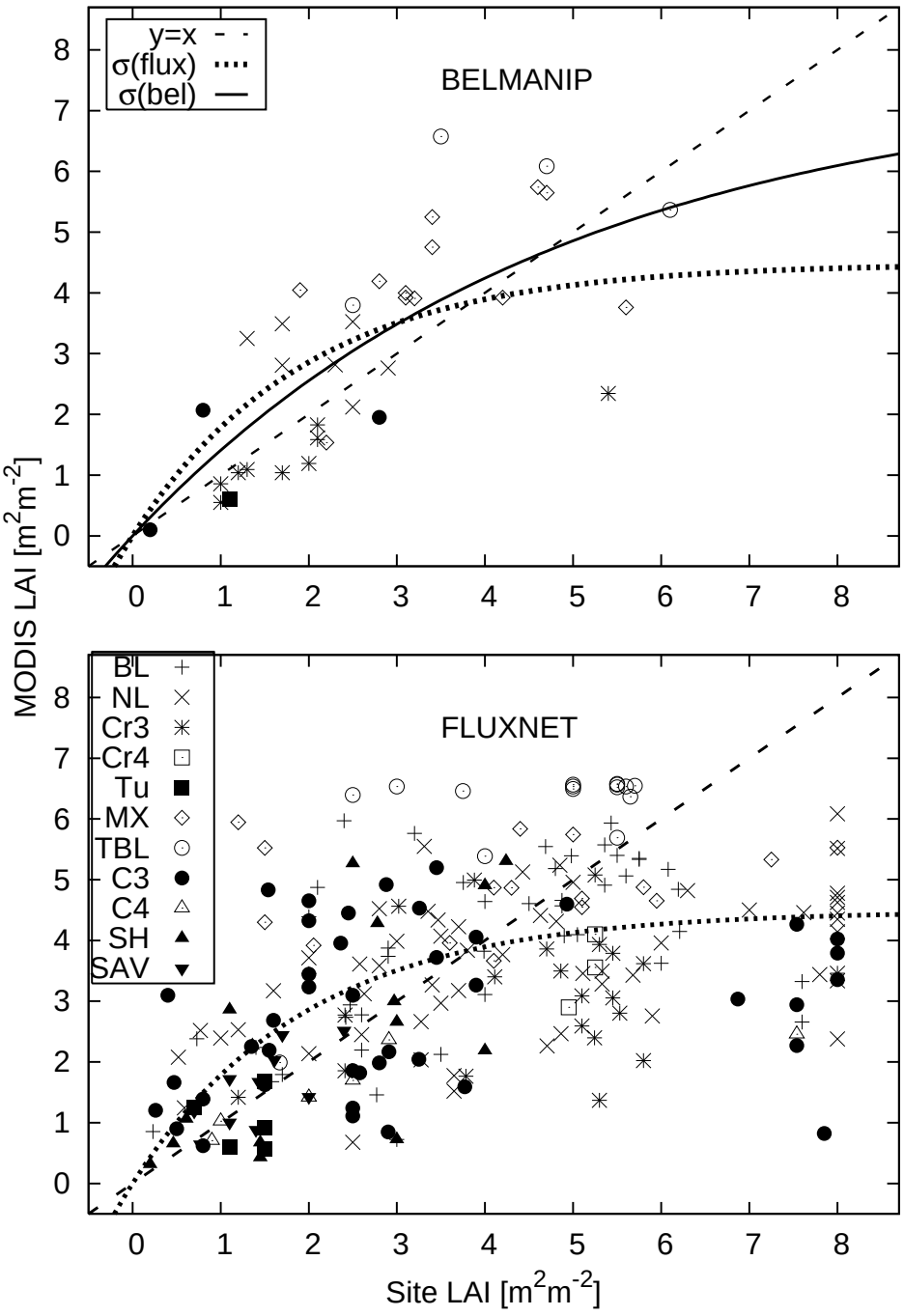

Figure 5: Barcharts comparing the interquartile range of retrieved $V_{cmax}^{25,toc}(grow)$, designated as "retrieval" in the legend, with the corresponding field-based range for the upper canopy. The retrieval is for global land points whereas the field-based ranges are based on extensive compilations by Kattge et al (2009), Wright et al (2005) and Wullschleger (1993). Beerling & Quick (1995; BQ) is based on a single estimate per PFT. Values are grouped according to PFT. Note that the retrieved range for C_4 crops is shown with C_3 crops (no field measurements are available for C_4 crops).

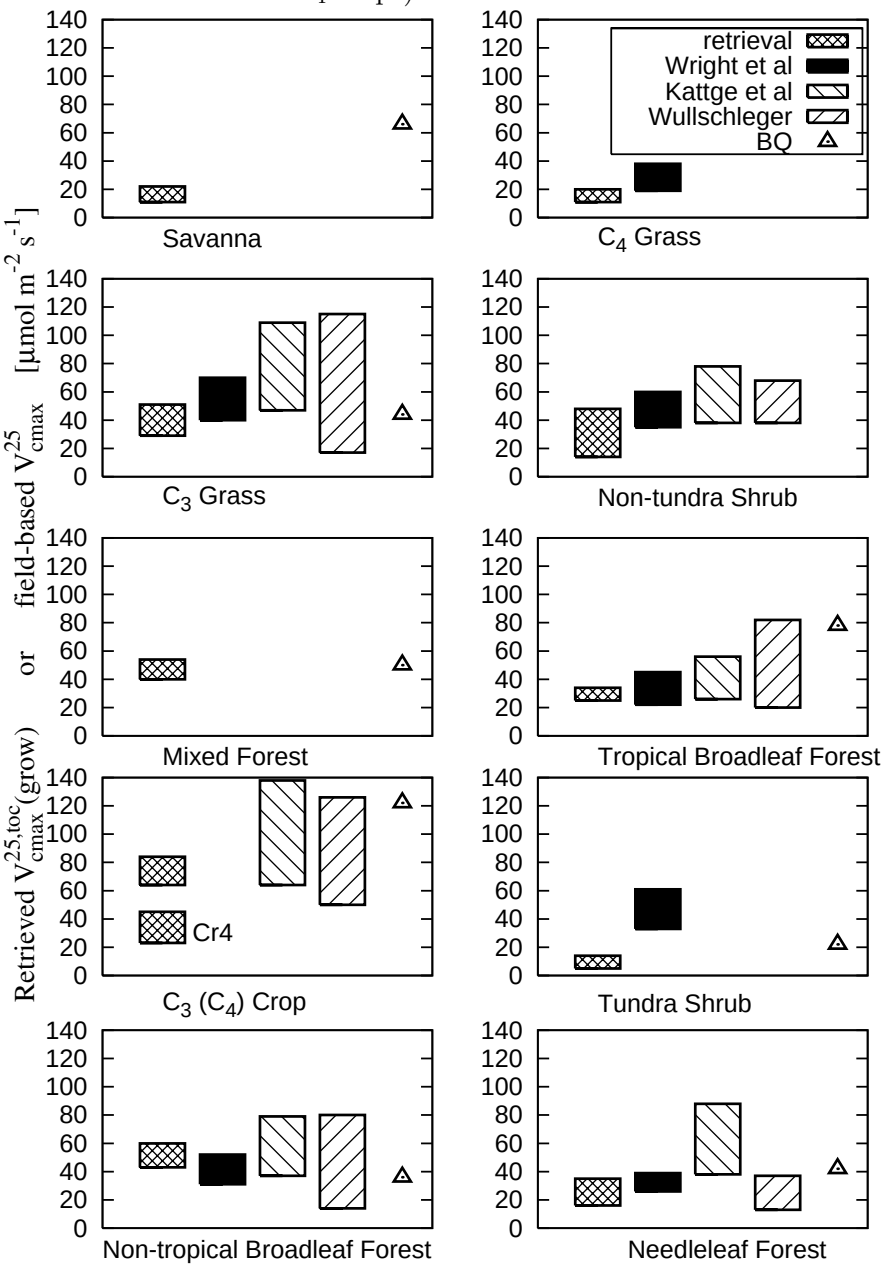

Figure 6: Zonal profile of retrieved maximum growing season light-limited and Rubisco-limited photosynthetic capacity ($J_{max}^{25,toc}(grow)$ and $V_{cmax}^{25,toc}(grow)$, respectively; lower panel) compared against land cover (upper panel). Land cover is represented as the percentage of total vegetation at each latitude and is compressed to basic life-forms (tree, grass/crop and shrub) for clarity.

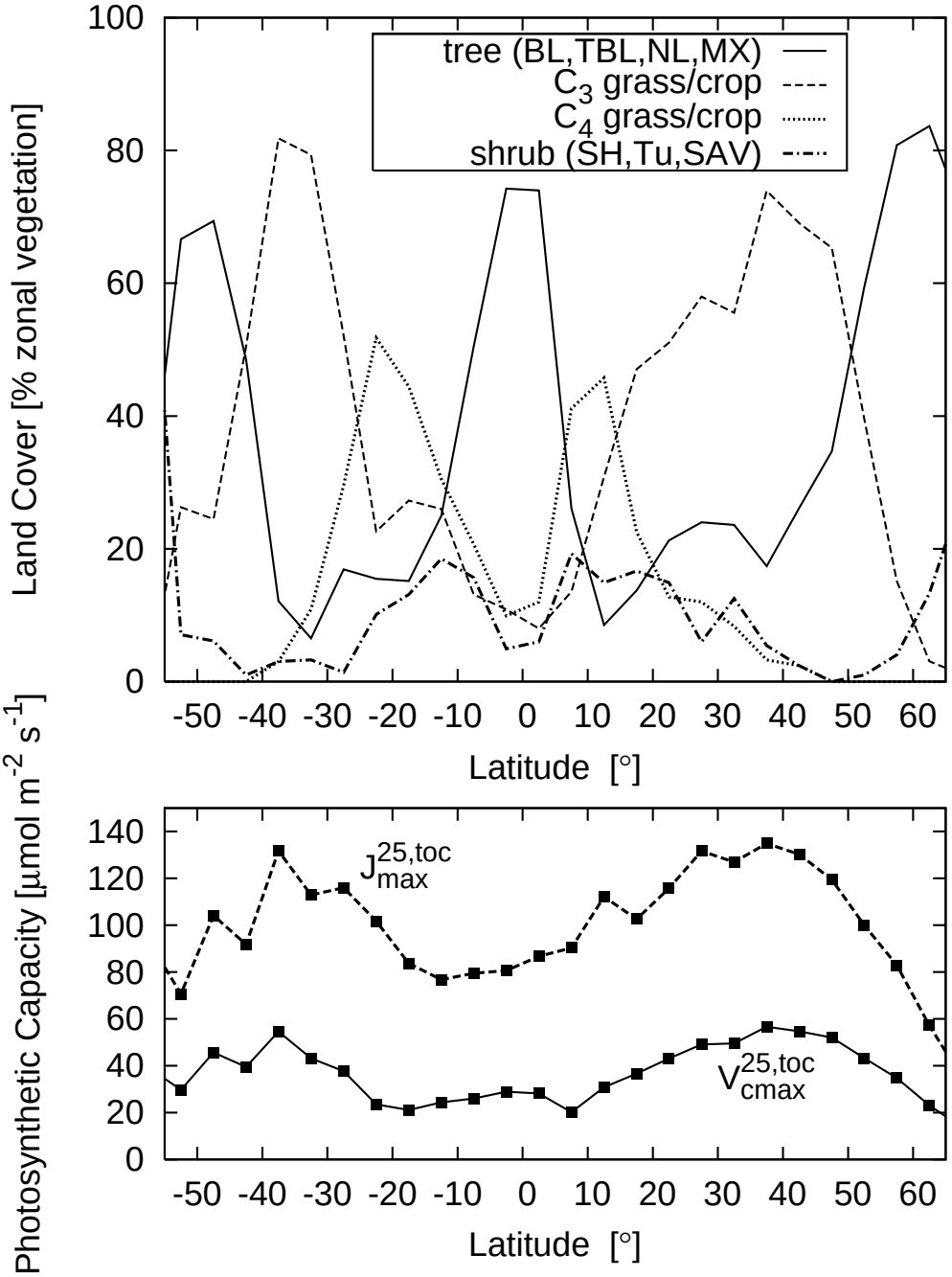

Figure 7: Maximum growing season photosynthetic capacity ($V_{cmax}^{25,toc}(grow)$; μmol m^{-2} s^{-1}) retrieved for 0.5° global grid-squares. Note that for locations of sparse vegetation (LAI<0.5 m^2 m^{-2}), a retrieval is not possible (black). This figure is reproduced in colour in the online version of this article.

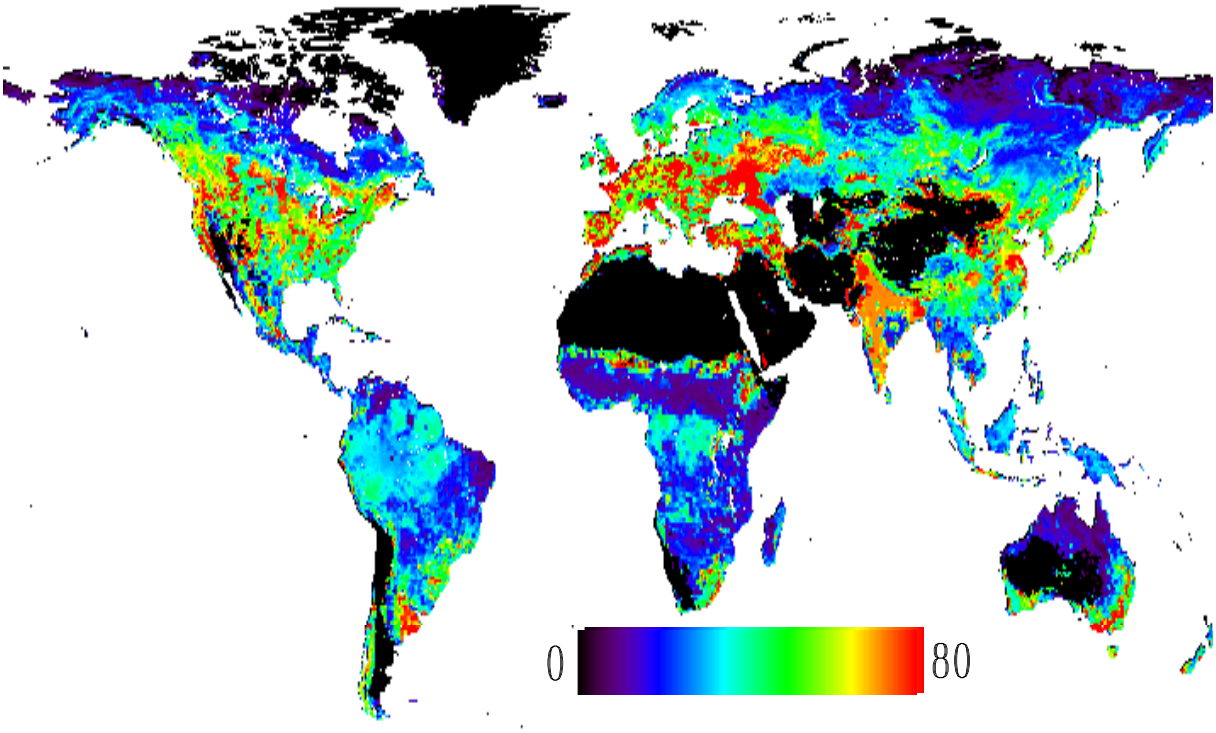

Figure 8: Global PFTs based on Goldwijk et al (2011) with modification according to the distribution of C_4 vegetation (Still et al 2003). Grid-squares are at 0.5° resolution. Land without vegetation is black. This figure is reproduced in colour in the online version of this article.

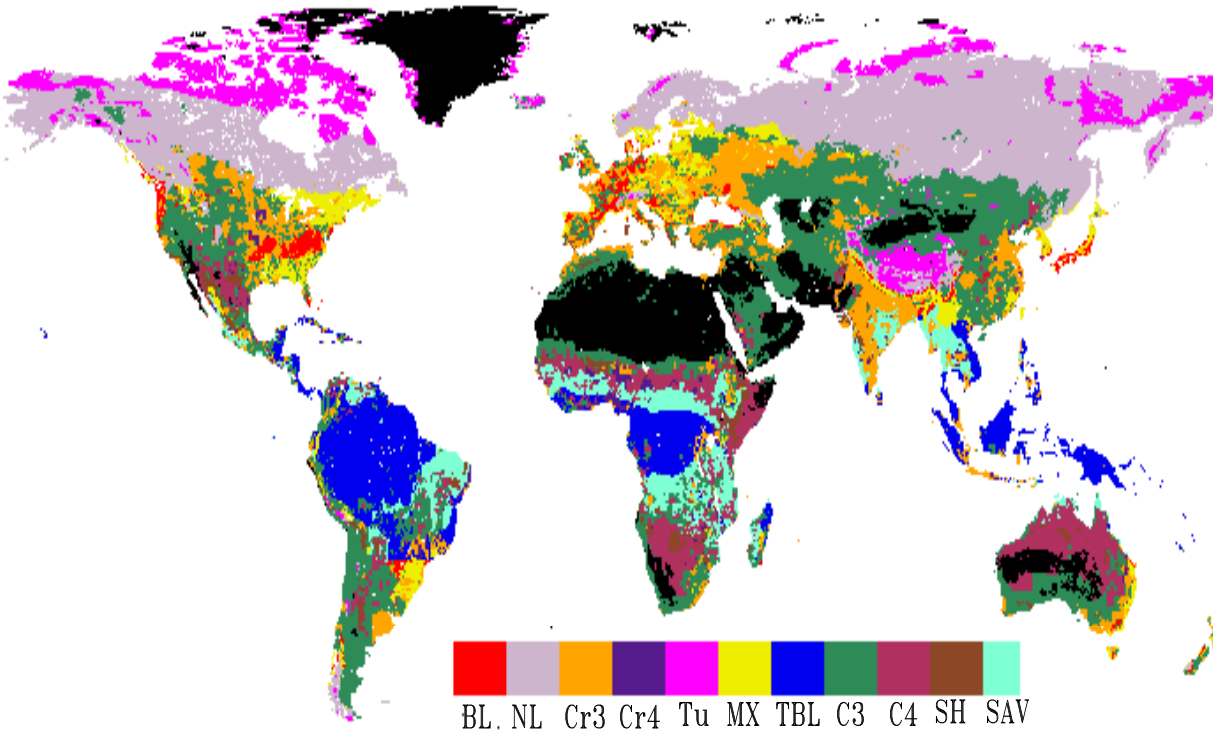

Figure 9: Trend in monthly $V_{cmax}^{25,toc}$ (solid) and LAI (dashed) anomalies for the period 2002-2012 for the northern (panel a) and mid-northern (panel b) latitudinal zones. Significant trends, where present, are fitted with a solid ($V_{cmax}^{25,toc}$) and a dashed (LAI) straight line (Tab. 5). Mean values averaged across the 2002-2012 period are shown as $< V_{cmax}^{25,toc} >$ and $< LAI >$. Note that LAI anomalies are in units of 0.1 m^2m^{-2} but $< LAI >$ is in units of m^2m^{-2}. The y-axis range (LAI) for the northern zone is twice that of the mid-northern zone.

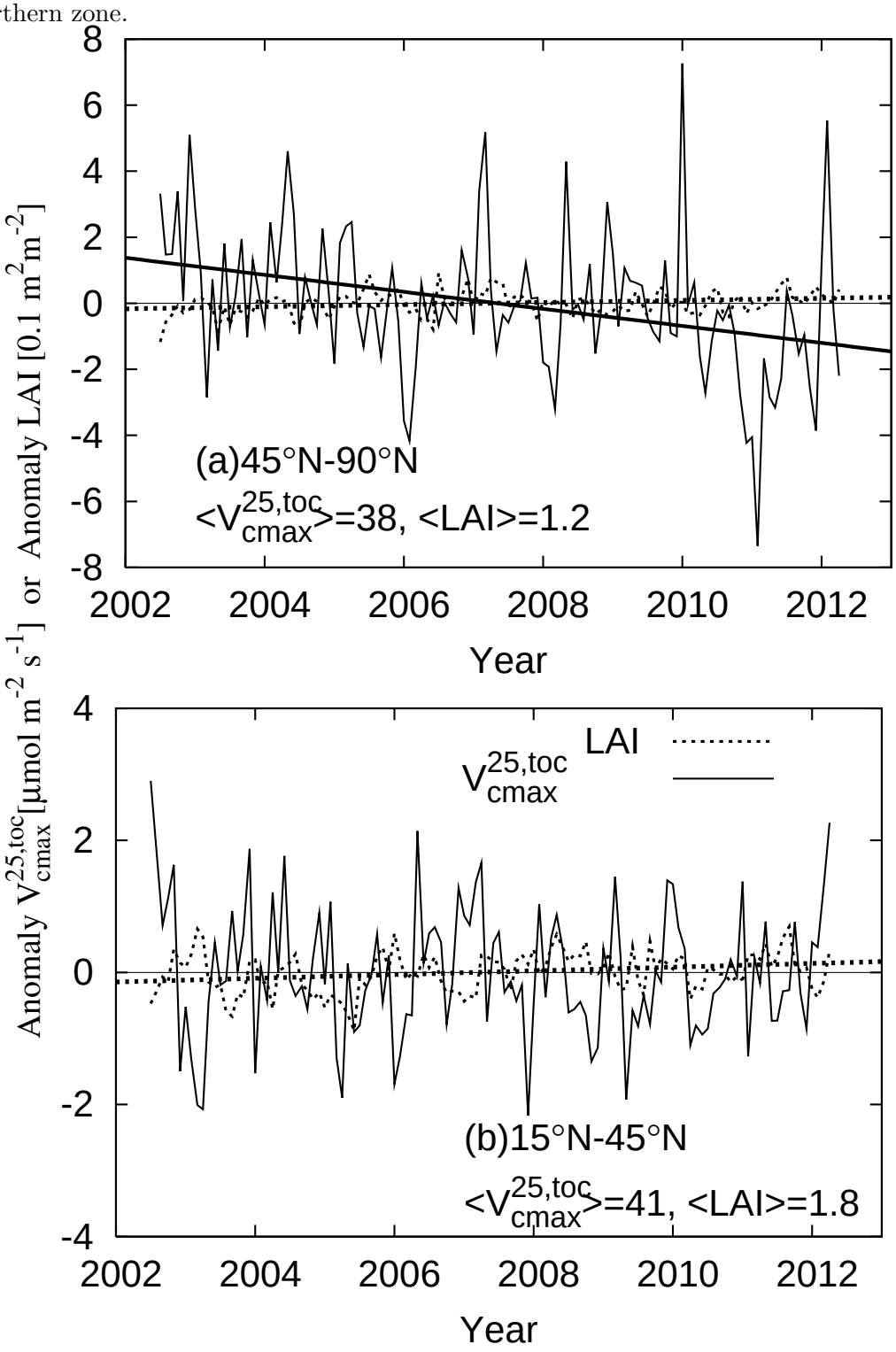

Figure 10: As Fig. 9 but for the tropics (panel a) and for the mid-southern zone (panel b).

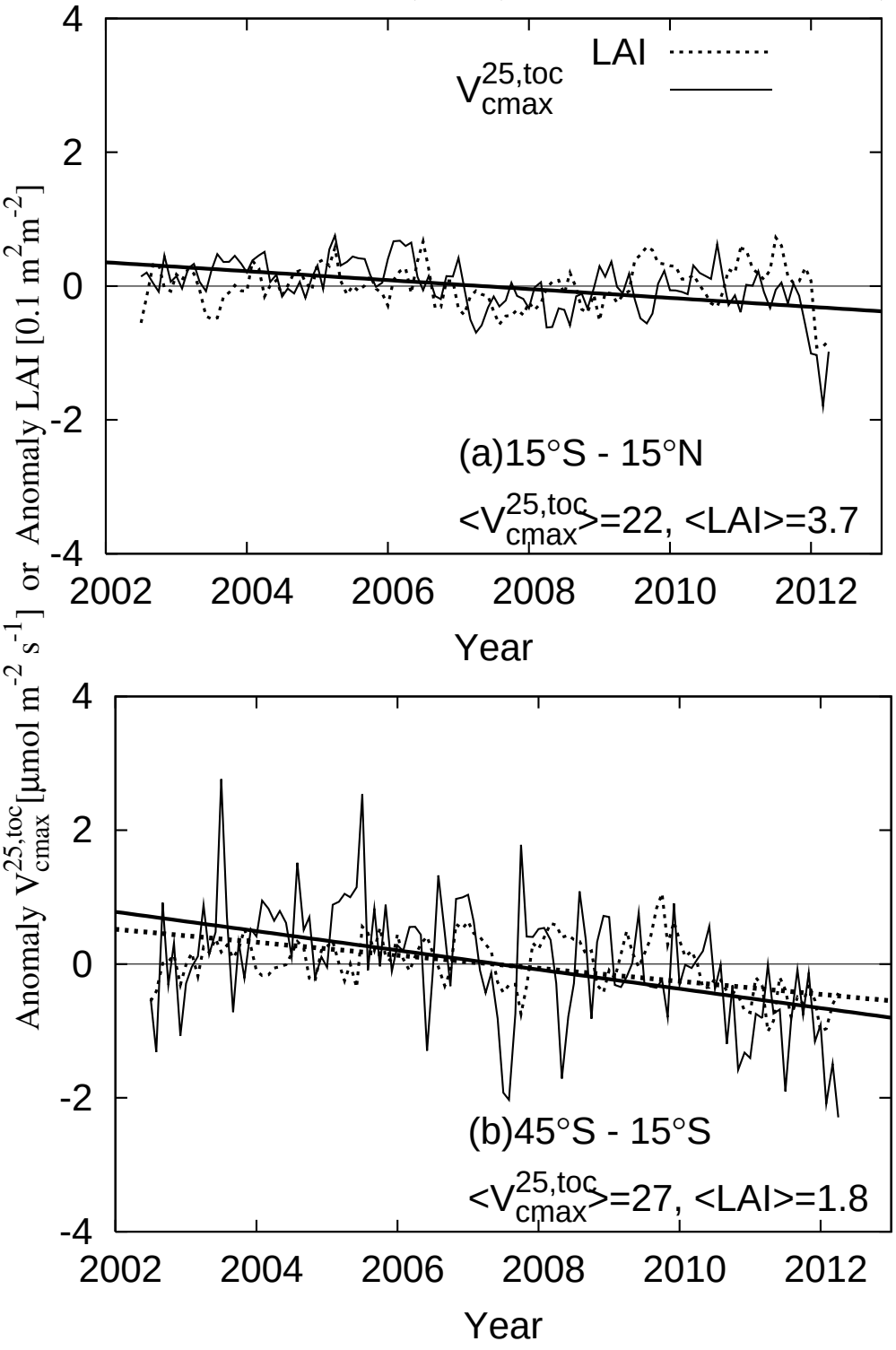

Figure 11: Decadal trends in monthly anomalies of $V_{cmax}^{25,toc}$ (squares with solid errorbars) and LAI (squares with dashed errorbars), shown separately according to global plant functional type. Plant functional types are abbreviated according to Tab. 3. Errorbars represent the standard error.

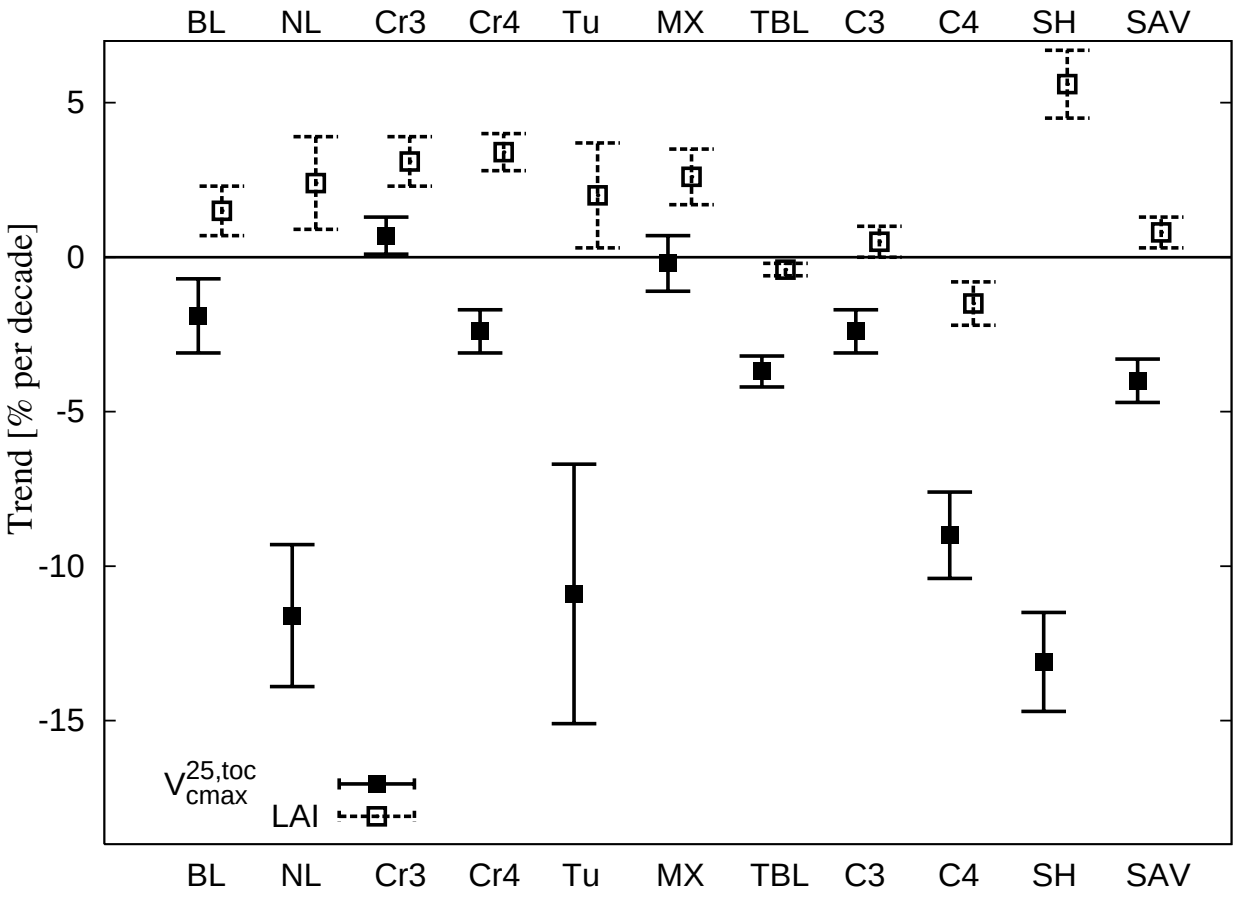

Figure 12: The decadal trend for the mid-northern (+15° to +45°) zone plotted against that for the combined tropics and mid-southern zone (-45° to +15°). The trend is defined for monthly anomalies in $V_{cmax}^{25,toc}$ (panel a) and LAI (panel b), expressed as a percentage of the mean value over the period 2002-2012. Each marker denotes a different plant functional type. Outliers are labelled using the abbreviations in Tab. 3. The y=x line and significant best fit ($V_{cmax}^{25,toc}$ only) are represented, respectively, by dashed and solid lines.